THERMALLY DRIVEN REFLUX IN FRACTURED POROUS MEDIA

by
Ronald T. Green and James D. Prikryl
Center for Nuclear Waste Regulatory Analyses
6220 Culebra Rd.
San Antonio, TX 78238 USA
rgreen@swri.edu

ABSTRACT

Heat generated by high-level nuclear waste (HLW) at the proposed geologic repository at Yucca Mountain, NV has been viewed as a means to dry out the repository environment and maintain the waste packages dry for long periods of time. However, there is potential that condensed water vapor could combine with infiltration water and form a saturated or near saturated zone above the repository. Refluxing of this water into the heated drift could lead to increased exposure of waste packages to water, thereby accelerating waste package failure and release of radionuclides into the geosphere. Results from laboratory-scale experiments designed to examine the refluxing phenomenon were compared with numerical simulations and an analytical solution of water flow through a heated fracture. The experiments provided evidence that water refluxing down fractures was able to penetrate the boiling isotherm and enter the heated drift. Predictions of the magnitude of refluxing by a dual matrix-fracture continua numerical model and the analytical solution were consistent with the experimental results.

INTRODUCTION

The United States Department of Energy (DOE) is evaluating the disposal of high-level nuclear waste (HLW) in a geologic repository located in unsaturated fractured rock at Yucca Mountain, a semiarid desert mountain in southern Nevada. Maintaining the HLW at dry conditions for long periods of time is a design objective for the repository [DOE, 1996]. Heat generated by the radioactive decay of HLW has been proposed as a mechanism that will dry out rock near the waste to maintain the repository environment at dry conditions for long periods of time [Buscheck et al., 1995]. A zone of saturation or near saturation, however, may form above the repository horizon as a result of infiltrating water and condensate from vaporized rock water [Ofoegbu et al., 1998; Bagtzoglou et al., 1998; Buscheck et al., 1994]. There is potential that water from this zone can flow down fractures and penetrate the dry-out zone created by the

heat-generating waste, increase the relative humidity of the repository environment, and wet the waste package, thereby accelerating corrosion of the waste packages [Pruess, 1997; Green and Prikryl, 1998, 1999; NRC, 1999]. This process could lead to earlier waste form degradation and release of radionuclides into the geosphere. Water accumulated on the heater apparatus during two field-scale heater tests - the Climax heater test [Patrick, 1986] and the 1988-89 G-Tunnel heater test [Buscheck et al., 1991; Ramirez, 1991; Lin et al., 1991] - lends credence to the hypothesis of refluxing at a geologic repository during periods of heat generation by the HLW.

The refluxing phenomenon has been evaluated with analytical, numerical, and physical models. An analytical solution by Phillips [1994, 1996] describes the theoretical depth that gravity-driven liquid water can penetrate beyond a boiling isotherm in partially saturated, fractured, porous media. This depth of penetration is mostly a function of the downward flux of water and the temperature gradient in the zone through which the penetrating water is flowing. Numerical simulations of flow through heated fractured porous media have been limited by the level of detail that can be assigned to the medium. Results from recent isothermal and nonisothermal field-scale tests have contributed to understanding thermally driven moisture flow through fractured, porous media. Isothermal tests allow examination of basic flow through partially saturated fractured media in the absence of the coupled effects caused by heating. Of particular interest are the Exploratory Studies Facility (ESF) isothermal niche studies conducted as part of the Yucca Mountain project [Wang et al., 1997, 1998; Hardin, 1998]. The information gained from these studies is critical to establish an understanding of flow into a drift in the absence of heat or during the period after heat has dissipated. Heater tests conducted at field scale, such as the Fran Ridge large block test (LBT) [Wilder et al. 1998, Lin et al., 1998], the ESF single-heater test [Tsang et al., 1998], and the ESF drift-scale heater test [Busheck et al., 1997; Hardin, 1998], provided valuable information on the effect of heat on the mechanisms that control reflux through fractured, porous media under nonisothermal conditions. Although very useful in discerning the nature of heat and mass transfer through partially saturated geologic media, field-scale tests have limitations in interpretation because of natural heterogeneity and measurement uncertainty.

Controlled laboratory-scale experiments were conducted in this study to reduce the uncertainty inherent

in field-scale experiments and to provide additional insights of thermally driven refluxing through a fractured, porous medium. The laboratory-scale experiments were conducted with consideration that flow and transport mechanisms observed in a synthetic medium of reduced size may not scale directly to the field, but appreciating the fact that laboratory-scale experiments can have controlled initial and boundary conditions and a medium that is more easily quantified than a field setting. Laboratory-scale experiments are viewed as complementary and not as replacements to tests conducted at field scale.

EXPERIMENTAL DESIGN

A laboratory-scale experimental apparatus was assembled, and two experiments, Tests 1 and 2, were conducted to observe moisture redistribution around a heat source located in a fractured, porous medium. The assembly of the apparatus was the same for both experiments. The experimental apparatus was a 1.2×1.2×0.6–m test cell assembled with solid rectangular (0.05×0.05×0.60 m) cast concrete blocks (Figure 1). The concrete blocks were fabricated from a mixture of bentonite clay, barite, and portland cement. The concrete blocks had the following measured property values: permeability of 2.0×10^{-17} m^2, total porosity of 0.50, thermal conductivity of 0.5 W/m-K (dry) and 1.0 W/m-K (wet), and van Genuchten α of 6.36×10^{-7} Pa^{-1} and n of 0.7619 [Green et al., 1995]. The van Genuchten α and n are fitting parameters for the moisture retention curve. Saturation of two samples of the concrete was measured prior to Test 1 to be 0.15 and 0.20. For Test 2, each of the concrete blocks was submerged in a bath of water–repellant sealant (Prime a Pell© by Chemprobe) to reduce the tendency for water to imbibe from the fractures into the blocks. The sorptivity of the concrete blocks was reduced from 1.6×10^{-4} $m\text{-}s^{-1/2}$ to 7.5×10^{-6} $m\text{-}s^{-1/2}$ by the application of the sealant. The spaces between the blocks were intended to mimic horizontal and vertical fractures. Fracture properties, which were not measured, were initially estimated and then refined during modeling calibration. A 0.15–m long, 0.019–m diameter cylindrical heat source was placed horizontally in a simulated (0.15–m diameter) drift centrally located in the test cell. Water was infiltrated into the top of the test apparatus through a 0.30–m long, 0.025–m diameter porous cylinder.

The concrete blocks were confined in an open-sided solid aluminum loading frame (Figure 1). The open sides of the test cell were covered with lexan plates. To reduce heat loss through the side walls, the lexan was covered with a 0.013–m thick layer of styrofoam for insulation in Test 1 and a 0.03–m thick blanket of

fiberglass insulation in Test 2. A 0.005–m thick rubber sheet was placed between the concrete blocks and confining aluminum plates at the top, bottom, and lateral sides of the test cell. A 0.01–m thick layer of sponge neoprene was placed between the lexan side walls and the concrete blocks to prevent both liquid and vapor flow at the boundaries. A compressive stress of 1,100 kg/m^2 was uniformly applied to the opposing ends of the test cell using cables, thus compressing the vertical fractures separating the individual concrete blocks. Approximately 680 kg was placed on top of the cell (equivalent to a 940 kg/m^2 compressive stress) to compress the horizontal fracture spacings in Test 1. The 680–kg mass was replaced in Test 2 with a compressive stress of 730 kg/m^2 applied with cables.

Horizontally oriented, water-contact sheets (divided into eight individually measured segments or panels) were used to detect dripping into the drift (Figure 2). The drip sensors were constructed of two 0.15 × 0.30–m sheets of Kapton® polymide film. Each sheet contained four of the eight drip–sensor panels. Each panel consisted of a copper-tin integrated circuit imprinted onto the sheets. The integrated–circuit system was designed to send an electrical signal when water or another electrical conducting substance came in contact with the sheets and closed an electrical circuit. In Test 1, the drip–sensor sheets were placed in an upward concave configuration slightly above the heater to allow any liquid that gathered on the sensors to be captured. An insufficient quantity of water was available to collect for testing in Test 1, therefore, the drip–sensor sheets were placed horizontally in the mid-plane of the drift in Test 2. Gas pressure and humidity in the drift were measured in both tests using a pressure transducer and a Humicap® psychrometric sensor. A thermocouple was installed in the Humicap® but was only operational for temperatures less than 100°C. Two additional thermocouples were installed in the drift in Test 2 to measure air temperatures in excess of 100°C. The two thermocouples were installed about 0.11 m into the drift, one positioned above the drip–sensor sheet and one below.

Temperature was measured in the media of the test cell using 100 thermocouples strategically placed along the vertically oriented fracture coplanar to the axis of the drift (referred to as the primary fracture) and in additional fractures throughout the test cell in Test 1.The 100 thermocouples were repositioned in only two vertically oriented planes in Test 2, one plane in the primary fracture and the second in one-half of a plane perpendicular to the primary fracture in the middle of the test cell. The locations of

thermocouple placement in the primary fracture for Tests 1 and 2 are illustrated in Figure 3. Note the greater density of measurement provided by thermocouple placement in Test 2. With this instrumentation, liquid flow at locations that were initially above boiling could be detected using thermocouples when downward moving water depressed the temperature to below boiling. This same technique was used during the field-scale Fran Ridge LBT [Wilder et al., 1998] to detect liquid flowing down fractures. Temperature measurements were taken once or twice daily during Test 1 and hourly during Test 2.

The heater was set at approximately 142 watts in both tests, calculated from measurements of 80 volts at the power source and 1.78 amps and 44.4 ohms through the heater. Tap water from a carbonate aquifer was introduced at a rate of 1,000 ml/day (equivalent to about one drop every 2 seconds) into the porous cylinder placed over the primary fracture at the top of the test cell to simulate the natural sources of water (i.e., infiltration and condensed water that originated from vaporized rock water) and allowed to infiltrate downward toward the heat source. Difficulties were encountered in Test 1 when the porous wall of the infiltration cylinder became clogged, presumably with carbonate precipitated from the tap water. The porous cylinder used for infiltration was replaced every four weeks during Test 2 to prevent clogging of the cylinder walls with carbonate precipitates. This procedure successfully eliminated clogging of the infiltration cylinder in Test 2 with the exception of one occasion near day 110 when the stopper at the end of the cylinder became dislodged, presumably as a result of clogging the cylinder, causing infiltration at a point rather than along a line. The tap water used for infiltration in Test 2 was modified by increasing the silicon concentration of the infiltration water. The spiked waters experienced a decrease in calcium and an increase in sodium by the addition of silicon. Although not entirely representative of water from the unsaturated zone at Yucca Mountain, the modified water more closely approximated Yucca Mountain water which is in equilibrium with siliceous tuff. One sample of pure tap water and two separate samples of the modified infiltrating water were analyzed. Results of these analyses are summarized in Table 1.

An effort was made to sample the water outflow from the test cell. However, only minor uncollectable amounts of water were observed during Test 1. A significantly greater quantity of water was available for collection from points of outflow from the test cell during Test 2. Water was sampled from a point of outflow at the base of the test cell on two occasions during Test 2 (days 121 and 146) and analyzed.

Results of the analyses are included in Table 1.

Test 1 ran for a total of 140 days–5 days of heating only followed by 125 days of heating and infiltration, culminating with 10 days of infiltration during a ramp-down of the heat source. Test 2 ran for a total of 215 days–again with 5 days of heating-only followed by 167 days of constant heating and infiltration but ending with 43 days infiltration with a ramp-down of the heat source. The heat source was incrementally and linearly decreased from 142 watts at day 167 to 36.8 watts at day 215, at which time the test was terminated. There was a brief power outage for about 20 hrs at day 153 of Test 2.

RESULTS

Test 1

The temperature of the heater was maintained at 475-510 °C for the 130-day duration of constant heating in Test 1. Most of the large variation in temperature measured at the heater (~35°C) is attributed to a slight movement of the thermocouple placed against the heater canister surface. Although elevated above waste package surface temperatures expected at the HLW repository according to DOE Viability Assessment design criteria [TRW Environmental Safety Systems Inc., 1998], this temperature was required to advance the boiling isotherm to a distance of 0.05 – 0.10 m into the concrete blocks. Within the blocks, a maximum temperature of 202 °C was observed in Test 1 at a distance of 0.0125 m into a fracture immediately below the heater. Above the heater, a maximum temperature of 175 °C was observed at the drift surface in the crown of the drift in the center of the cell. Contours of temperature measured in the primary fracture after 10, 50, and 110 days of heating are illustrated in Figure 4a. Note that only half of the primary fracture surface is illustrated because most of the thermocouples in the fracture in Test 1 were located in that half of the fracture [Figure 3(a)]. Inspection of temperatures measured at selected thermocouples in the other half of the primary fracture confirmed that heat flow, at least in the primary fracture, was approximately symmetric prior to the onset of infiltration.

Temperatures observed in the primary fracture after the onset of infiltration in Test 1 were, at times, nonsymmetric. This nonsymmetry is illustrated in Figure 5a, which plots the locations of the boiling

isotherm (i.e., 99°C for the elevation at which the experiment was conducted) at days 10, 20, 30, 50, 70, 90, and 130 of the test. The highest temperatures were achieved after 10 days of heating and 5 days of infiltration. Thereafter, temperatures decreased, and the boiling isotherm migrated downward toward the heater. Of interest is the nonuniform downward advance of first the right side, second the left side, and finally the middle portion of the isotherm. Due to the spatial (eight thermocouples evenly spaced over a horizontal distance of 0.355 m) and temporal (two readings per day) coarseness of measurement, it is possible that narrow, episodic ribbons of water may have advanced down fractures toward the heater and evaded detection. Movement of the boiling isotherm stalled at a distance of 0.04 m above the drift at day 50, and it remained essentially stationary for the duration of the experiment.

Temperature and relative humidity measured in the air space of the drift midway between the end of the drift and the end of the heater for Tests 1and 2 are plotted versus time in Figures 6 and 7. Although the temperature measurements suggested stabilization of the wetting front by day 50 of the experiment, relative humidity measured in the drift continued to increase for an additional period of time. After decreasing to an overall low of 14 percent at day 12, relative humidity increased to a high of about 60 percent at day 108. Several momentary declines in relative humidity were recorded during the experiment. A stoppage in infiltration due to clogging of the infiltration system experienced at days 46-47 and 59-60 of the experiment correlated well with the first two declines in relative humidity. The cause for the more prominent decrease in relative humidity after day 110 may be a consequence of a longer term reduction in infiltration that occurred prior to being detected at day 124. Air temperature at the end of the drift was steady at about 90-95°C after the first ten days of the test. The 5°C decrease in drift-air temperature at day 62 was due to a repositioning of the drift-air thermocouple located in the relative–humidity sensor.

The test assembly and concrete blocks were disassembled at the conclusion of Test 1. Visual inspection of the concrete blocks revealed a precipitate deposited on fracture surfaces proving that water flowed along fracture pathways. The precipitate was determined, using x-ray diffraction (XRD), to be composed mostly of aragonite ($CaCO_3$) and calcite ($CaCO_3$). This composition compares to an XRD analysis of the pretest concrete that identified barite ($BaSO_4$), calcite, gismondine ($CaAl_2Si_2O_8 \cdot 4H_2O$), kaolinite-

montmorillonite [$Na_{0.3}Al_4Si_6O_{15}(OH)_6 \cdot 4H_2O$], and moganite ($SiO_2$) as the dominant minerals. Formation of aragonite and calcite on fracture surfaces was expected because these carbonate minerals have retrograde solubility [e.g., their solubility decreases with increases in temperature over the temperature range of interest (e.g., 25 to 200°C)]. Flow through fractures, evidenced by the presence of the precipitate on fracture surfaces, was restricted to a zone that emanated from the area of infiltration and expanded laterally in a parabolic shape as it flowed downward and eventually extended to a width of about 0.15 m beyond the sides of the drift. It was not possible to discern whether flow down the fractures exhibited sheet-flow or channelized-flow characteristics. Although the concrete blocks were noticeably wet outside this fracture flow zone, there was no indication of liquid flow down fractures outside this zone because of the absence of minerals deposited on fracture surfaces.

Electrical responses provided by the drip sensors during Test 1 were ambiguous. The drip–sensor sheets became dislodged during an adjustment of the drift temperature probe at day 62 and came into contact with the heaters. The four middle segments of the two sheets incurred heat damage by partial melting and emitted misleading signals thereafter. As a result of this ambiguity, the electrical responses of all sensors were considered questionable for the duration of the experiment. Visual observation through the lexan plates and inspection of the drip sensors after the completion of Test 1 indicated that dripping into the drift occurred during heating and not during the 10-day cooling period at the end of the experiment. Although the precipitate was concentrated at the ends of the drip sheets, residual precipitate was present on the drip sheets throughout the drift with the exception of a 0.14–m span that included half the heater and 0.04 m beyond that end of the heater (Figure 8a). As illustrated in photographs of the post-test drip sensors from Test 1, the central portions of the sheets were damaged because of their proximity to the heater. Of greater interest is the evidence of precipitate deposition over 75 percent of the entire length of the drift and, in particular, the total corrosion of the drip sensor (noted at the right end of the photograph), which was induced by the precipitate deposition and possibly by high temperature and moisture conditions. Two samples of precipitates were collected from the drip sensors – one from an area where the precipitate color was tan and one from an area where the color was dark brown – and analyzed using XRD. Aphthitalite [$K_3Na(SO_4)_2$], barite, and calcite were detected in both samples, with aphthitalite most abundant in the tan sample and barite most abundant in the dark brown sample. Aphthitalite and barite

contain the same components used to fabricate the concrete blocks. Calcite, on the other hand, is likely derived from both the composite of the concrete blocks and the infiltrating water, whose source is a carbonate aquifer. It is noteworthy that these three minerals typically act as electrical insulators, not conductors, which diminished the usefulness of the electrical-contact sheets to detect dripping.

Test 2

Temperatures in Test 2 differed from those observed in Test 1 even though the heater power and test cell assembly were the same. The temperature of the heater in Test 2 was maintained at 440-485 °C for the 172-day duration of full heating of the experiment. As stated previously, the variation in temperature measured at the heater was mostly attributed to minor repositioning of the heater thermocouple. Within the blocks at a distance of 0.0125 m into a fracture immediately below the heater, a maximum temperature of 452 °C was observed. It should be noted that the heater rested more directly on the concrete blocks in Test 2 than in Test 1. A maximum temperature of 175 °C was observed at the drift surface in the crown of the drift in the center of the cell above the heater. Contours of temperature measured in the right half-plane primary fracture after 10, 50, and 175 days of heating are illustrated in Figure 4b.

As also noted in Test 1, temperatures observed in the primary fracture in Test 2 were nonsymmetric, although with different asymmetry than observed in Test 1. This nonsymmetry is illustrated in Figure 5b which shows a plot of the locations of the boiling isotherm at days 10, 50, 90, 110, 150, 175, 190, 200, and 210 of the test. Similar to Test 1, the highest temperatures were achieved after ten days of heating and five days of infiltration. However, contrary to Test 1, a monotonic decline in temperature was not observed in Test 2 results. In Test 2, the boiling isotherm dropped to a minimum height of about 0.03 m above the right side of the top of the drift at about days 110 to 125. By day 140, the boiling isotherm retreated upward on the right of the drift but dropped on the left. After the boiling isotherm encroached toward the drift on the right side of the primary fracture for a period of about 15 days (until day 125), it was discovered that the stopper at the right end of the 0.30–m long porous infiltration cylinder (i.e., above that portion of the boiling isotherm that encroached on the drift ceiling) had become dislodged, thereby focusing the infiltration water down the right side of the primary fracture. As illustrated in Figure 5b, the

boiling isotherm regained symmetry after the infiltration cylinder was replaced, and infiltration was again applied evenly over the 0.30–m span. With the exception of this localized deviation, the boiling isotherm nearly became stationary toward the end of the heating period but never completely stalled as observed during Test 1. The minimum distance separating the boiling isotherm from the drift was about 0.04 m at the end of the heating period, similar to Test 1.

The spatial and temporal resolution of measurement was more refined in Test 2 than Test 1. In Test 2, it is possible that a narrow ribbon of water that advanced down fractures toward the right side of the drift around days 110 and 125 is indicated in the boiling isotherm plot (Figure 5b). A plot of temperatures recorded at specific individual thermocouples provides further illustration of cooling associated with water refluxing down a fracture. In particular, the rapid reduction of temperature at day 115 from about 130 to 100°C at thermocouple No. 56 illustrates cooling from rapid fracture flow (Figure 9). Thermocouple No. 56 is located in the primary fracture about 0.012 m above the drift ceiling. The episodic nature of the fracture flow is illustrated by the ensuing dryout (i.e., rapid increase in temperature from 100°C back to 130°C) at days 123, 143, and 148 with each event quickly followed by rapid rewetting. Similar activity was observed at other themocouples (for example, No. 45 located 0.05 m from the primary fracture at the same elevation of the drift and No. 63 located in the primary fracture about 0.025 m above No. 56) whose rapid temperature fluctuations above and back to boiling also strongly suggested rapid, episodic fracture flow (Figure 9). The temperature at No. 63 eventually decreased below boiling after day 92 suggesting the continued presence of liquid water in the fracture.

The drift-air temperature and relative humidity for Test 2 are plotted versus time in Figures 6 and 7. The temperatures and relative humidity differed significantly between Tests 1 and 2 although the heat source strength and infiltration rates were the same in both tests. The drift-air temperature above and below the drip sensor in Test 2 approached 180°C and 210°C, compared with the below boiling drift-air temperatures in Test 1. Temperatures in Test 2 were more erratic than in Test 1. In addition, the drift-air temperature in Test 2 demonstrated a gradual decrease (i.e., ~1.5°C/week above the drip sensors and ~2 K/week below the drip sensor) through the end of the experiment after initially experiencing a somewhat more dramatic increase (i.e., ~5°C/week for the first 4 weeks after an initial week of rapid

heating) at both drift thermocouples for the first five weeks of the test. Relative humidity decreased from 80 percent at the start of Test 2 to about 5 percent within the first week then erratically increased to about 10 percent at the time heating was reduced. Relative humidity increased rapidly to over 75 percent when the drift-air temperature decreased below boiling.

The test assembly and concrete blocks were disassembled at the conclusion of Test 2. Of interest was the presence of standing water on the top surface of many of the concrete blocks, particularly on the top surfaces of blocks located near the cooler outer boundaries. Precipitate observed on fracture surfaces at the conclusion of Test 2 could not be solely attributed to either Test 1 or Test 2, therefore post-test inference of flow along fracture pathways during Test 2 was not possible. An XRD analysis of the precipitate deposited on the Test 2 drip sensors detected aphthitalite and barite (constituent minerals in the concrete) as the most abundant minerals. There was no evidence of calcite on the Test 2 drip sensors. Although the total amount of precipitate deposited on the drip sensors in Test 2 appeared less than the amount deposited during Test 1, the number of occurrences and extent of corrosion of the drip sensors in Test 2 exceeded that observed in Test 1.

Upon completion of the inspection of the test cell at the conclusion of Test 2, the concrete blocks were sampled from two planes perpendicular to the drift. Approximately 20 concrete samples were collected from each plane in the test cell to measure the saturation. One sampling plane was located in the middle of the test assembly and the other near the assembly outer edge. Measured saturations of the samples from these two planes are presented in Figure 10. As illustrated, saturations of samples from the middle of the test cell provide a coherent rendering of the moisture status of the matrix of the blocks at the conclusion of Test 2. Measured saturations of samples collected at the outer edge of the test cell provided a less coherent picture of moisture at the boundary. The noise in the data at the edge is attributed to nonuniform heat and mass transfer along the boundaries.

Inspection of the drip shields at the conclusion of Test 2 revealed that three of the middle drip–sensor segments incurred significant damage from the heater during the test. However, in the absence of prolonged or continuous electrical signals from the drip sensors, there is no indication that the heat

damage resulted in errant drip signals. As indicated in Figure 11, electrical responses from the drip sensors in Test 2 provided evidence of dripping during the heating phase of the experiment. The responses are plotted in terms of relative voltage. Both the strength and locations of responses varied. Several events or event groups were observed in the sensor results. All events are attributed to dripping. In the first event group, dripping was observed at both ends of the drift during the first two to three weeks of the experiment. The second event group consisted of dripping into the middle and right half of the drift, which was observed for about 30 days starting at day 90 of the experiment. Several individual electrical responses were detected late in the experiment, but prior to the rampdown of the heater. One event, in particular, occurred in the middle of the drift and lasted for about 10 days.

ANALYSES

Thermally driven reflux down fractures toward the heat source was evaluated using results from the two laboratory-scale experiments, an analytical solution, and a numerical model. Of particular interest to this evaluation are the differences in responses observed between Test 2 and Test 1.

Laboratory Analysis

Interpretation of heat and mass transfer in the test cell was made using temperature measurements, direct and indirect moisture assessments, and chemical analyses from the tests. Although there was a high level of similarity in the responses of Tests 1 and 2, there were significant differences between observed drift-air temperatures. The drift-air temperatures of Test 1 appeared to be inconsistent with the measured matrix temperatures. Test 1 drift-air temperatures were consistently below boiling although adjoining matrix temperatures were above boiling. The source of the temperature differences was investigated. There is no evidence of temperature measurement error during the tests. The thermocouples were calibrated prior to the tests and were within ±1 K at the conclusion of both tests. The temperature and relative humidity readings were consistent for both tests supporting the accuracy of the temperature measurements. The maximum attainable relative humidity diminished markedly below 100 percent for temperatures above boiling. For example, the maximum relative humidity possible at 150 and 200°C is about 21.4 and 6.6 percent. Relative humidity for temperatures above boiling is defined as the partial pressure of moisture in air divided by the saturation vapor pressure of water at same dry-bulb

temperature [Worrall, 1965]. Relative humidity values of 65 and 10 percent are consistent at drift-air temperatures of about 90 °C in Test 1 and 180 to 210 °C in Test 2. Therefore, there is no evidence to support the supposition that Test 1 drift-air temperatures were in error. The low drift-air temperatures are believed to be bonafide and controlled by heat and mass transfer between the matrix and fracture continua.

Although episodic fracture flow was observed at several locations throughout the test cell (i.e., Figure 9), episodic fracture flow into the drift was not detected using thermocouple temperature measurements taken in the primary fracture during either test. Precipitate deposition on the drip sheets during both tests provided firm evidence that water did flow into the drift. As illustrated in Figure 4a, temperature measurements from Test 1 indicated that the boiling isotherm advanced in a uniform, albeit, segmented fashion but never collapsed into the drift until heating was decreased after day 130. The width of each of the three segments was about 0.10-0.20 m. Temperature measurements do not indicate that dripping water entered the drift during the heating phase of the experiment. Contrary to the temperature measurements, dripping into the drift was indicated by precipitate deposited on the drip–sensor sheets. Observations through the lexan side walls during both tests substantiate that the precipitates were deposited during the heating phases of the experiments. In Test 1, precipitate was found in about 75 percent of the entire drift and 50 percent of the drift containing the heater, although most of the precipitate was deposited away from the heater at the ends of the drift. Although the temperature of the drip–sensor sheets was high (above boiling through part of the drift length), there were indicators that the sludge-like precipitate flowed for some distance (i.e., as much as 3 cm) across the inclined surface of the drip sensor before drying [Note locations of drops indicted in Figures 8(a) and (b)]. Although the drip–sensor precipitate covering was not as thick in Test 2 as in Test 1, there was evidence that precipitate was present at various locations throughout the entire length of the sensors in Test 2 [Figures 8(c) and (d)].

The post-test sorptivity of the concrete blocks was measured to be 7.5×10^{-6} m-s$^{-1/2}$, a decrease by a factor of 20 from the untested pretest, concrete sorptivity values. This suggests that the fractures and matrix had more rapid hydraulic communication during Test 1 than Test 2. Under Test 1 conditions, only fractures located in zones where the concrete blocks were fully saturated appeared to have flow. This

hypothesis is consistent with the absence of carbonate precipitate on fracture surfaces except within the zone of infiltration in the central portion of the test cell. However, it is postulated that the matrix was more actively involved in flow during Test 1 than during Test 2. This level of activity may have declined in the region of active fracture flow during Test 1 as precipitate was deposited on the fractures exposed to flow. In Test 2, it is assumed only fractures allowed water flow partly because of the sealant applied to the concrete blocks prior to Test 2 and the saturation of the blocks was possibly higher at the onset of Test 2 than Test 1, thereby reducing the capillary driving force causing water to imbibe into the matrix.

Chemical analyses of the infiltration water, pretest concrete, and precipitate deposited on the fracture and drip-sensor surfaces during the tests provide additional insight into the flow mechanisms active during Test 1. Because the Test 1 concrete blocks were reused in Test 2, it was not possible to ascertain what chemical deposition could be attributed to Test 2. Therefore, fracture coating analysis was restricted to Test 1. Drip-sensor-precipitate analysis, however, included both Tests 1 and 2. An XRD analysis indicated that the precipitate that formed on the concrete fracture surfaces during Test 1 was composed of calcite and aragonite. The chemical components of these $CaCO_3$ phases likely originated mostly from both components of the concrete (i.e., calcite and gismondine) and from infiltration water that contained both Ca^{2+} and HCO_3^- . On the other hand, the sulfate-bearing precipitate that formed on the drip sensor surfaces in Tests 1 and 2 derived their components predominantly from dissolution of concrete. This suggests that the reflux water spent adequate time in contact with the concrete blocks (although the vertical distance from the point of infiltration to the top of the drift was only 0.43 m) to acquire elevated concentrations of Na^+, K^+, Ba^{+2}, and $SO4^{-2}$, which eventually led to the formation of aphthitalite and barite inside the drift. At no time during either test was there sufficient water on the drip sensors to allow water sample collection for analysis. Therefore, the consistency and concentration of the water that dripped into the drift cannot be definitively ascertained, but the nature of the drip trackings on the drip sensors [see points A, B, C, and D in Figures 8(a) and (b)] suggests that the drips had a sludge-like consistency and, presumably, relatively high concentration levels of the minerals deposited in the precipitates.

There was no evidence of standing water on the top surface of the concrete blocks during the disassembly of the test cell at the conclusion of Test 1. The presence of standing water on the concrete

block fracture surfaces after Test 2 qualitatively suggests the sealant applied to the blocks at the conclusion of Test 1 effectively reduced concrete imbibition such as experienced during the first test. These observations are consistent with the measured decrease in sorptivity resulting from the application of the sealant to the concrete blocks. The sealant caused the matrix and fracture continua in Test 2 to act separately compared to Test 1 during which the two continua had increased hydraulic equilibrium.

Analytical Solution

Analytical expressions describing infiltration of a liquid finger or ribbon down a fracture into superheated rock were developed by Phillips [1996]. Phillip's analysis is predicated on heat moving from the rock medium by thermal diffusion into the fracture causing liquid water flowing down an open fracture to evaporate. The depth that a ribbon of water will penetrate down a fracture past a preexisting boiling isotherm in a rock medium is dependent on the rate of the downward moving water, the rate that heat diffuses through the rock matrix, and the temperature gradient at the location of the boiling isotherm. Heat is assumed to flow into the water ribbon from a distance of order $(\alpha_t t)^{/2}$, where α_t is the thermal diffusivity of the rock and t is time. Therefore, the cooled volume of rock around the ribbon is of order $bl(\alpha_t t)^{1/2}$, where b is the width of the ribbon and l is the penetration distance below the boiling isotherm (Figure 12). Heat of order $(\rho_r C)_m \nabla T bl(\alpha_t t)^{1/2}$ is extracted from the rock to boil the ribbon of water in time t where ρ_r is the density, C is the heat capacity of the rock matrix, and ∇T is the temperature gradient at the lowest extent of the penetrating water ribbon. Equating the heat required to boil the mass of water entering the fracture with the heat extracted from the rock and solving for the depth of penetration gives

$$l_{early}(t) \approx \left[\left(\frac{\rho_f Q_o h}{\kappa_m \nabla T} \right) \frac{(\alpha_t t)^{\frac{1}{2}}}{b} \right]^{\frac{1}{2}} \qquad (1)$$

where ρ_f is liquid density, h is enthalpy, Q_o is the volume of water per unit time, and κ_m is thermal conductivity, and with a geometric stipulation that $(\alpha_t t)^{1/2} \leq b$. For longer times of order $(\alpha_t t)^{1/2} > b$, the cooled region around the ribbon becomes circular, and the depth of penetration becomes

$$l_{late}(t) = \left(\frac{\rho_f Q_o h}{K_m \nabla T} \right)^{\frac{1}{2}} \qquad (2)$$

Equations 1 and 2 can be applied to Tests 1 and 2. Parameter values valid for both experiments are :

$\alpha_t = 6.0 \times 10^{-7}$ m^2/s,

$\rho = 1 \times 10^3$kg/m^3,

$h = 2.35 \times 10^6$ W-s/kg,

$k_m = 0.7$ W/m-K, and

$Q_o = 1.1 \times 10^{-8}$ m^3/s.

The temperature gradient at the boiling isotherm located above the heat source is estimated from temperature measurements to be 770 K/m (50°C change over 0.065 m). Sufficient latitude in choosing a representative temperature gradient justifies using 770 K/m for both tests. Neither Equation (1) or (2) are sensitive to changes in sorptivity, therefore predictions of penetration of the boiling isotherm made with this analytical solution will be the same for Test 1 and 2. Stated differently, the Phillips solution (1994, 1996) does not account for imbibition of water from fractures into the matrix.

Equation (1) is valid for transient times up to steady conditions, and equation (2) applies thereafter. Steady water penetration conditions are estimated after 1.7 days according to the thermal diffusion length criterion. Using these assigned values, the depth of penetration of the boiling isotherm at late time is calculated with Equation (2) to be 0.21 m.

Numerical Analysis

The test cell was numerically modeled using MULTIFLO [Lichtner and Seth, 1998], a nonisothermal, multiphase simulator. The tests were individually simulated to reflect differences in hydraulics between the tests (i.e., matrix/fracture interactions). Both experiments were simulated by treating the test volumes as two continua, fractures and matrix, commonly referred to as a dual continuum model (DCM) [Pruess, 1991; Lichtner and Seth, 1998]. The DCM conceptualization provides a separate continuum for both the matrix and the fractures joined throughout the model domain by transfer functions to effect heat and mass transfer between the two continua.

The transfer of fluid between continua is analogous to Darcy's law in which the rate and direction of fluid transfer is a function of the pressure difference between the two continua, the surface area interfacing the two continua, and the harmonic mean of the matrix and fracture hydraulic conductivities. This fracture-matrix coupling can be expressed as

$$Q_t = \frac{\sigma_f A_{mod} \rho g}{\mu} k_{harmonic} k_r \frac{P_f - P_m}{d} \quad (3)$$

where g is gravity, μ is viscosity, k_r is the upstream weighted relative permeability, P is pressure, and d is the distance over which the fracture-matrix pressure drop occurs. The variable σ_f is a composite measure of the fraction of bulk volume occupied by fractures and matrix block size, and A_{mod} is a modifier used to characterize the connectivity between the fracture and matrix continua. Reducing A_{mod} has the effect of decoupling the two continua. The harmonic mean of hydraulic conductivity at the fracture/matrix interface is defined as

$$k_{harmonic} = \frac{k_f k_m}{k_f + k_m} \quad (4)$$

An analogous form of Fouriers law is used to define the rate of transfer of heat between the matrix and fracture continua.

The test cell was numerically modeled in three dimensions. Vertical symmetry in two dimensions justified modeling one-fourth of the test cell. Material properties were assumed uniform throughout the test cell and assigned values from actual measurements for the concrete matrix [Green et al., 1995] and from estimations for the fractures. Dry and wet thermal conductivity values were reduced from the measured unfractured thermal conductivity values of 0.5 and 1.0 W/m-K to 0.4 and 0.7 W/m-K for the concrete matrix, to be consistent with the fractured nature of the multiple blocks. Comparable relative values for tuff gravel and intact tuff support this property value modification [Green et al., 1997] External boundaries were specified as no fluid flow, but with some heat flow (loss). Thermal properties assigned to the

boundaries to effect heat loss were determined by matching numerically predicted temperatures with observed temperatures at 5 and 10 days of heating (i.e., prior to effects from infiltration) and at 110 days (i.e., the effects of both heating and infiltration were included). Greater heat loss through the bottom of the test cell relative to the top of the test cell was indicated during the calibration process. This heat loss is attributed to the large mass of aluminum that formed the base of the test cell. The heater strength was reduced by 10 percent to adjust for heat loss through the heater assembly. The drift was modeled as a highly permeable fractured medium and was assigned a thermal conductivity value of 10 W/m-K to indirectly account for radiative heat transfer through the air space.

The only parameter values that differed between the models for Tests 1 and 2 were the values assigned to the dual continua coupling term, A_{mod}, and the initial saturation although modifications in values assigned to other model properties were assessed. Values for A_{mod} were uniformly varied for all elements from unity (fully coupled and large matrix-fracture cross-sectional area) to 10^{-6} (mostly decoupled or reduced matrix-fracture area due to channelized flow) for both models. Saturations of the test matrix at the onset of Test 1 and the conclusion of Test 2 were measured, however saturations at the conclusion of Test 1 and the start of Test 2 were not measured and had to be inferred. Initial saturations for Test 2 were modified to achieve the best agreement between simulations and matrix saturations measured at the conclusion of Test 2 and matrix temperatures measured throughout the test. This calibration process was inherently complicated because of the coupled relationship between mass (water) and heat transfer. Best agreement between simulated and measured temperatures was achieved in Test 1 when a value of 10^{-2} was assigned to A_{mod}. Best agreement for Test 2 was achieved with a value of 10^{-4} assigned to A_{mod} and an initial saturation of 0.32. Although this saturation is less than that postulated (not measured) at the onset of Test 2, agreement between the final measured saturation and the predicted saturation suffered if higher initial Test 2 saturations were assumed. Final model values for Tests 1 and 2 are summarized in Table 2. Numerically simulated matrix and fracture temperatures for Test 1 at 10, 50, and 110 days are presented in Figures 13 (a) and (b). The halfplanes are oriented coplanar to the primary fracture. Similarly, matrix and fracture temperatures for Test 2 are presented for days 10, 50, and 175 in Figures 14 (a) and (b). The relative humidity predicted for the fracture and matrix continua of the drift are presented for Tests 1 and 2 in Figures 15 (a) and (b). Matrix saturations simulated after the conclusion of

Test 2 at the edge and along the mid-plane of the test cell are presented in Figure 16 for comparison with the measured final saturations (Figure 10) in the same plane.

DISCUSSION

The refluxing phenomenon was evaluated using experimental evidence, an analytical solution, and numerical simulation. According to the analytical solution for penetration of the boiling isotherm by Phillips [1994, 1996], water should be available to enter the heated drift in slightly less than two days after the time when downward flowing liquid water first encounters the boiling isotherm above the crown of the drift. The cause for the short time required for penetration of the boiling isotherm is attributed to two possible causes. First, the Phillips model does not incorporate the effects of water imbibition from fractures into the matrix. Second, the relatively dry initial conditions under which this Test 1 was conducted may have precluded a response as rapid as predicted by Phillips [1994, 1996]. The time to achieve steady conditions is believed to be greater in Test 1 than predicted by the Phillips solution due to the high porosity (0.50) and low initial saturation (15 - 20 percent) of the concrete blocks at the onset of the experiment. The surfaces of the concrete blocks used in Test 1 were absent of materials resembling fracture coatings, therefore, unimpeded imbibition consumed much of the infiltrating water prior to water being available for fracture flow at greater depths within the medium. Conversely, the fracture surfaces of the concrete blocks in Test 2 were modified to impede the rate of imbibition, however insufficient evidence was available to compare actual rates of fracture flow in Test 1 to that in Test 2. In addition, the temperature gradient could only be roughly estimated and is equally appropriate for analyzing both tests. The predicted steady-state depth of penetration of 0.13 m is thereby applicable to Tests 1 and 2.

Numerical simulations of Tests 1 and 2 were evaluated to interpret the results of the laboratory-scale experiments, assess the accuracy of the analytical solution for penetration of the boiling isotherm, and help formulate a credible conceptual model of thermally driven reflux in fractured porous media. The DCM capability of the numerical simulator was particularly useful to evaluate variations in heat and mass transfer between the matrix and fracture continua observed in Tests 1 and 2. The lack of complete coupling specified between the matrix and fracture continua caused simulated temperatures and saturations to differ between the matrix and fracture continua. Although matrix and fracture temperatures

were somewhat similar throughout most of the test cell in Test 1, fracture temperatures above the heater were depressed relative to matrix temperatures (i.e., the boiling isotherm was closer to the drift in the fracture continuum than in the matrix continuum). The boiling isotherm penetrated about 0.07 m (i.e., 0.47 to 0.53 m from the top of the test cell) below the fracture relative to the matrix. In fact, the simulated boiling isotherm dropped below the level of the top of the drift (i.e., 0.52 m) suggesting dripping into the drift. It appears that the model successfully incorporated sufficient flow down a fracture to depress temperatures in the fracture and allow liquid to reach the drift.

The increased decoupling of the matrix and fracture continua (or decrease in matrix-fracture cross-sectional area) in Test 2 (i.e., $A_{mod} = 10^{-4}$) led to higher temperatures at the drift than predicted for Test 1 with less decoupling (i.e., $A_{mod} = 10^{-2}$). These elevated drift temperatures are consistent with Test 2 results. Decoupling of the two continua in Test 2 was sufficiently high to allow enough water to flow down the primary fracture so fracture temperatures did not exceed boiling until late in the simulation (i.e., between 150 and 175 days). Test 2 simulations indicated that the fracture boiling isotherm never penetrated into the rock mass above the drift, therefore, the depth of penetration of the boiling isotherm was 0.07 m - the difference between the maximum depth of the boiling isotherm into the rock matrix (0.45 m) predicted for Test 2 and the top of the drift (0.52 m).

One significant departure of the simulations from the experimental results was that neither simulation predicted that the boiling isotherm would initially advance to a maximum distance into the medium before collapsing to a reduced distance prior the end of the experiment. This mechanism was observed in both Tests 1 and 2. A numerical model with the properties of Test 1 was used to predict the location of the boiling isotherm in the absence of infiltrating water. This simulation (not shown here) indicated that the maximum extent of the boiling isotherm was 0.44 m, or only slightly greater than indicated by the matrix temperature of the Test 2 simulation. It is interesting to note that the boiling isotherm location in the matrix was the same as in the fracture continuum in the simulation with no infiltration. Although infiltrating water reduced the distance that the boiling isotherm advanced into the medium when compared to simulations with no infiltration, the simulations with infiltration never predicted a greater distance from the drift to the boiling isotherm than the final predicted distance.

A second significant departure of the simulations from the experimental results was that the episodic nature of dripping during refluxing was not captured by the numerical models. Strong evidence of episodic dripping was provided by thermocouple measurements in fractures that exhibited large rapid changes in temperature. These rapid temperature fluctuations are interpreted to indicate rapid cooling by the arrival of water at a thermocouple located in an environment at above-boiling temperatures or rapid heating due to drying of water in an environment that was otherwise above boiling. Electrical responses of the drip sensors and the deposition of precipitate on the sensor sheets provided additional direct evidence of dripping during the heating phase of the experiments although the rate of water flow could not be quantified with this evidence. The discrete, discontinuous data acquisition frequency of either the thermocouple or the drip-sensor measurement technique failed to detect the true spatial and temporal frequency of dripping in the cell. The extent of precipitate deposition on the drip sensors did provide an approximate cumulative record of the drift area exposed to dripping over the full duration of each experiment.

There was general agreement between simulated and measured saturations along the midplane of the test cell but somewhat less agreement at the edge of the test cell. Nonetheless, both measured saturation cross sections indicated elevated saturation above the heater and a dryout zone below. The elevated saturation zone above the heater in Test 2 was near full saturation and was attributed to the combination of infiltration water flowing down and from the condensation of water vapor rising up. Simulated saturation values (Figure 15) were neither as high above the heater nor as low below the heater compared to measured saturation (Figure 10). Elevated saturation which was measured along the edge at the base of the test cell and confirmed with the observed dripping from the base during Test 2, was not indicated in the simulations. It should be noted that mass sinks were not explicitly incorporated into the numerical model, however, the manner in which heat sinks were accommodated did result in limited additional mass storage at the boundaries. Nonetheless, the heat sinks were incorporated by specifying an elevated heat capacity for boundary elements where heat was lost from the test cell. In this way, water that dripped out of the test cell in both tests, but more excessively in Test 2, was incorporated into the model while maintaining a reasonable mass balance within the test cell volume.

For both tests, values of relative humidity predicted for the drift were consistent with the predicted temperatures, but only marginally in agreement with drift-air relative humidity observed during the experiments. In Test 1, drift-air temperatures were predicted to be in excess of boiling for both continua for the duration of the experiment even though measured drift-air temperatures never exceeded boiling. The cause for this inconsistency is not known particularly in light of the fact that the same humidity sensor used in Test 1 was also used in Test 2, which detected neither values of anomalously high relative humidity nor low temperatures. In both Test 1 and 2 simulations, the relative humidity was consistent with each respective temperature. Predicted relative humidity was low when the temperature exceeded the boiling isotherm as expected. Likewise, for temperatures below the boiling isotherm, as was the case in the fracture continuum in Test 2, the relative humidity was at 100 percent until near day 200 when the temperature exceeded boiling resulting in a rapid decline in relative humidity. It is noteworthy that the decline in temperature associated with the decrease in heater power in Test 2 (Figure 6) was not captured well in the numerical model. Consequently, an increased relative humidity related to the decreased temperature during the cooling phase of Test 2 was not wellrepresented in the model.

CONCLUSIONS

Results from laboratory-scale experiments indicated that dripping into a cavity heated to above boiling temperatures can be experienced even if an apparent zone of above boiling temperature exists above the cavity. Direct evidence for the dripping during the experiments was the presence of precipitate deposited on drip sensors located in the drift during two similar, but separate, experiments and direct evidence of dripping into the drift from drip-sensor measurements in the one experiment (i.e., Test 2) in which the drip sensors were operational. Additional evidence of episodic dripping down fractures was provided by periodic temperature measurements at thermocouples located throughout the test cell. Rapid decreases or increases in temperature are evidence of liquid water momentarily depressing the temperature in an environment that is otherwise at above boiling temperatures. Fluctuations in temperature measurements taken in fractures at 10-minute increments during a larger-scale, fractured-rock experiment at Fran Ridge [Wilder et al., 1998] was interpreted to indicate episodic liquid flow down fractures.

The principal source of the precipitate deposited on the drip sensors in the drift appeared to be minerals dissolved from the concrete medium, as well as calcite from the carbonate infiltration water. The principal difference between the two tests was the degree of imbibition, or sorptivity, of water into the concrete blocks that formed the test cell. Test 2 exhibited a factor of 20 decrease in sorptivity in response to the application of a sealant to the concrete block surfaces after Test 1, but prior to Test 2.

Simulation of the experimental results was accomplished using a DCM conceptualization in which hydraulic connectivity between the fracture and matrix continua was impeded, but not fully decoupled. The degree of coupling was reduced from Test 1 to Test 2 to achieve the best agreement with laboratory results. This suggests that the sealant applied to the fracture surfaces after the conclusion of Test 1 and prior to Test 2 had the effect of further reducing the hydraulic communication between the fractures and matrix and increasing the time required for hydraulic equilibrium to be established between the two continua. Lastly, the presence of a zone above the drift with temperatures in excess of boiling did not preclude continued increasing levels of relative humidity in the drift during Test 1 even after the downward migration of the boiling isotherm stalled.

The depth of penetration of the boiling isotherm was calculated using an analytical solution for the penetration of liquid water flowing down a fracture in heated rock [Phillips, 1994, 1996] and found to be about 0.13 m for both tests. The analytical solution does not account for either imbibition into the matrix or hydraulic coupling between the matrix and fracture continua. This prediction was compared with the depth of penetration predicted using MULTIFLO [Lichtner and Seth, 1998], a nonisothermal, multiphase simulator. A maximum depth of penetration of 0.06 m for Test 1 and 0.07 for Test 2 was predicted with the numerical model. The numerical predictions of penetration depth compared reasonably well with the experimentally observed distances determined using thermocouple measurements taken during both Tests 1 and 2. The predicted penetration depths were sufficiently large to allow dripping into the drift.

There were two significant departures of the numerical simulations from the experimental results. First, neither simulation predicted that the boiling isotherm would initially advance to a maximum distance into the medium before collapsing to a reduced distance prior the end of the experiment. This mechanism was

observed in both Tests 1 and 2. Second, the numerical models were not able to capture the episodic nature of dripping during refluxing. Strong evidence of episodic dripping was provided by thermocouple measurements in fractures that exhibited large rapid changes in temperature indicating the rapid arrival of water or drying of water in an environment that was otherwise above boiling.

Most importantly, however, electrical responses of the drip sensors and the deposition of precipitate on the sensor sheets provided direct evidence of dripping into the drift during the heating phase of the experiments. Water refluxing into emplacement drifts and onto waste packages, if present at a geologic HLW repository, could lead to accelerated HLW waste package corrosion as a result of the additional liquid water from dripping or increased relative humidity caused by dripping induced drift-air temperatures.

ACKNOWLEDGMENTS

This research was sponsored by the Nuclear Regulatory Commission (NRC) under Contract No. NRC-02-97-009. The activities performed were on behalf on the NRC Office of Nuclear Material Safety and Safeguards, Division of Waste Management. This paper is an independent product of the Center for Nuclear Waste Regulatory Analyses and does not necessarily reflect the views or the regulatory position of the NRC.

REFERENCES

Bagtzoglou, A.C., G.I. Ofoegbu, and R.T. Green. 1998. Thermally-driven moisture flow near the vicinity of perched aquifers in unsaturated geologic media. *Proceedings for the 12th International Conference on Computational Methods in Water Resources*. Crete, Greece. June, 1998.

Buscheck, T.A., R. Carlson, W. Daily, K.Lee, W. Lin, N. Mao, A. Ramirez, T. Ueng, H. Wang, and D. Watwood. 1991. *Prototype Engineered Barrier System Field Test (PEBSFT) Final Report.* UCRL-ID-106159. Livermore, CA: Lawrence Livermore National Laboratory.

Buscheck, T.A., J.J. Nitao, and L.D. Ramspott. 1995. Localized dryout: An approach for managing the thermal-hydrological effects of decay heat at Yucca Mountain. *Proceedings of the XIX International Symposium on the Scientific Basis for Nuclear Waste Management*. Pittsburgh, PA.: Materials Research Society.

Buscheck, T.A, R.J. Schaffer, and J.J. Nitao. 1997. *Pretest Thermal-Hydrological Analysis of the Drift-Scale Thermal Test at Yucca Mountain*. SP9318M4. Livermore, CA: Lawrence Livermore National Laboratory.

Green, R.T., F.T. Dodge, S.J. Svedeman, R.D. Manteufel, G. Rice, K.A. Meyer, and R.G. Baca. 1995. *Thermally Driven Moisture Redistribution in Partially Saturated Porous Media*. NUREG/CR-6348. Washington DC: Nuclear Regulatory Commission.

Green, R.T. , J.D. Prikryl, and M.E. Hill. 1997. Assessment of heat flow through bulk geologic material. *Proceedings of the 24th International Thermal Conductivity Conference*. Pittsburgh, PA. October 26-29, 1997. Technomic Publishing Co.

Green, R.T. and J.D. Prykryl. 1998. Penetration of the boiling isotherm by flow down a fracture. *Proceedings of the Third International Symposium on Multiphase Flow*. Lyon, France. June 8-12, 1998.

Green, R.T. and J.D. Prikryl. 1999. Formation of a dry-out zone around a heat source in a fractured porous medium. *Proceedings of the Second International Symposium on Two-Phase Flow Modeling and Experimentation*. Pisa, Italy. May 23-26, 1999. Edizioni ETS.

Hardin, E.L. 1998. *Near-Field/Altered Zone Models Report*. UCRL-ID-129179. Livermore, CA: Lawrence Livermore National Laboratory.

Lichtner, P.C. and M.S. Seth. 1998. *MULTIFLO Users Manual: MULTIFLO Version 1.2β Two-Phase Nonisothermal Coupled Thermal-Hydrologic-Chemical Flow Simulator*. San Antonio, TX: Center for

Nuclear Waste Regulatory Analyses.

Lin. W., A. Ramirez, and D. Watwood. 1991. *Temperature Measurements from a Horizontal Heater test in G-Tunnel.* URCL-JC-106693. Livermore, CA: Lawrence Livermore National Laboratory.

Lin, W., D. Wilder, S. Blair, T. Buscheck, W. Daily, G. Gdowski, W. Glassley, K. Lee, A. Mieke, A. Ramirez, J. Roberts, D. Ruddle, J. Wagoner, D. Watwood, T. Williams. R. Carlson, and D. Neubauer. 1998. An overview of progress on the large-block test of the ESF thermal tests. *Proceedings of the Ninth International High-Level Waste Management Conference*. LaGrange, IL: American Nuclear Society.

Nitao, J.J. 1988. *Numerical Modeling of the Thermal and Hydrological Environment Around a Nuclear Waste Package Using the Equivalent Continuum Approximation: Horizontal Emplacement*. UCID-21444. Lawrence, CA: Lawrence Livermore National Laboratory.

Nuclear Regulatory Commission. 1999. *Issue Resolution Status Report (Key Technical Issue: Thermal Effects on Flow) Revision 2.* September, 1999.

Ofoegbu, G.I., A.C. Bagtzoglou, R.T. Green, and M.A. Muller. 1998. Effects of perched water on thermally driven moisture flow at proposed Yucca Mountain repository for high-level waste. *Nuclear Technology.* Vol. 125. 235-253.

Patrick, W.C. 1986. *Spent Fuel Test - Climax: An Evaluation of the Technical Feasibility of Geologic Storage of Spent Nuclear Fuel in Granite. Final Report.* UCRL-553702. Lawrence, CA: Lawrence Livermore National Laboratory.

Phillips, O.M. 1994. Liquid infiltration through the boiling-point isotherm in a desiccating fractured rock matrx. *Proceedings of the Fifth International High-Level Waste Management Conference*. LaGrange, IL: American Nuclear Society. 2189-2196.

Phillips, O.M. 1996. Infiltration of a liquid finger down a fracture into superheated rock. *Water Resources Research.* 32(6):1665-1670.

Pruess, K. 1991. TOUGH2: *A general-purpose numerical simulator for multiphase fluid and heat flow.* LBL-29400, EC-251. Berkeley, CA: Lawrence Berkeley Laboratory.

Ramirez, A.L. 1991. *Prototype Barrier System Field Test (PEBSFT) Final Report.* UCRL-ID-106159. Lawrence, CA: Lawrence Livermore National Laboratory.

TRW Environmental Safety Systems Inc. 1998. *Total System Performance Assessment - Viability Assessment Analyses - Technical Basis Document.* B00000000-01717-4301-00001 REV 01.Las Vegas, NV: TRW.

Tsang, YW., J. Apps, J.T. Birkholzer, B. Freifeld, M.Q. Hu, J. Perterson, E. Sonnenthal, and N. Spycher. 1999. *Yucca Mountain Single Heater Test Final Report.* LBNL-42537. Berkeley, CA: Lawrence Berkeley National Laboratory.

U.S. Department of Energy. 1996. *Mined Geologic Disposal System Advance Conceptual Design Report*: B00000000-01717-5705-00027 Rev 00. Washington, DC: Office of Civilian Radioactive Waste Management. Department of Energy.

Wang, J.S.Y., R.C. Trautz, P.J. Cook, S. Finsterle, A.L. James, J. Birkholzer, and C.F Ahlers. 1998. *Testing and Modeling of Seepage into Drift: Input of Exploratory Study Facility Seepage Test Results to Unsaturated Zone.* Level 4 Milestone SP33PLM4. Berkeley, CA: Lawrence Berkeley National Laboratory.

Wang, J.S.Y., P.J. Cook, R.C. Trautz, R. Salve, A.L. James, S. Finsterle, T.K. Tokunaga, R. Solbau, J. Clyde, A.L. Flint, and L.E. Flint. 1997. *Field Testing and Observation of Flow Paths in Niches: Phase I Status Report of the Drift Seepage Test and Niche Moisture Study.* Level 4 Milestone SPC314M4. Yucca Mountain Site Characterization Project. Berkeley, CA: Lawrence Berkeley National Laboratory

Wilder, D.G., W. Lin, S.C. Blair, T. Buscheck, R.C. Carlson, K. Lee, A. Meike, A.L. Ramirez, J.L. Wagoner, and J. Wang. 1998. *Large Block Test Status Report.* UCRL-ID-128776. Livermore, CA: Lawrence Livermore National Laboratory.

Worrall, R.W. 1965. Psychrometric determination of relative humidities in air with dry-bulb temperatures exceeding 212°F. in Humidity and Moisture. Vol 1. *Principles and Methods of Measuring Humidity in Gases.* edited by A Wexler. New York, NY: Reinhold Publishing Corporation.

Table 1. Water quality analysis results (total alkalinity is mg $CaCO_3$/L), outflow sample (a) collected on day 121, outflow sample (b) collected on day 146

	tap water (mg/l)	spiked tap water (mg/L)	spiked tap water (mg/L)	outflow water[a] (mg/L)	outflow water[b] (mg/L)
aluminum	<0.05	<0.05	<0.05	5.74	4.56
barium	0.039	<0.005	0.006	0.097	0.127
calcium	66.0	5.53	7.89	1.58	2.56
iron	<0.02	<0.02	<0.02	0.114	0.120
magnesium	13.8	8.54	9.42	0.114	2.61
manganese	<0.005	<0.005	<0.005	<0.005	<0.005
phosphorous	<0.01	<0.01	<0.01	0.082	0.709
potassium	0.879	1.14	1.25	950	1500
silicon	5.68	75.3	74.1	83.6	91.3
sodium	8.44	147	160	406	675
strontium	0.395	0.063	0.080	0.017	0.020
sulfur	5.44	5.04	5.49	104	136
zinc	0.511	0.076	0.084	0.011	0.223
bromide	<0.2	<0.2	<0.2	<0.2	<0.2
chloride	16.2	15	15.2	20.1	62.2
phosphorous-P	<0.1	<0.1	<0.1	<0.1	0.336
sulfate	18.2	16.3	16.4	288	352

	tap water (mg/l)	spiked tap water (mg/L)	spiked tap water (mg/L)	outflow water[a] (mg/L)	outflow water[b] (mg/L)
pH	7.37	9.95	9.95	9.74	10.01
total alkalinity	190	220	250	394	665

Table 2. Property values assigned to the numerical model

Property	Test 1	Test 2
matrix porosity [-]	0.42	0.42
matrix permeability [m^2]	2.0×10^{-17}	2.0×10^{-17}
matrix density [kg/m^3]	1600	1600
matrix heat capacity [J/kg-K]	840	840
matrix α [Pa^{-1}]	6.37×10^{-7}	6.37×10^{-7}
matrix n [-]	1.59	1.59
fracture porosity [-]	0.05	0.05
fracture permeability [m^2]	1.0×10^{-10}	1.0×10^{-10}
fracture α [Pa^{-1}]	1.3×10^{-1}	1.3×10^{-1}
fracture n [-]	4.20	4.20
thermal conductivity - dry [W/m-K]	0.4	0.4
thermal conductivity - wet [W/m-K]	0.7	0.7
matrix sorptivity [$m\text{-}s^{-1/2}$]	2.0×10^{-17}	2.0×10^{-17}
matrix sorptivity with sealant [$m\text{-}s^{-1/2}$]	2.0×10^{-17}	2.0×10^{-17}
matrix initial saturation [-]	0.20	0.32

Property	Test 1	Test 2
matrix porosity [-]	0.42	0.42
fracture initial saturation [-]	0.01	0.01
σ_f [-]	0.05	0.05
A_{mod} [-]	1.0×10^{-2}	1.0×10^{-4}

FIGURES

1. Schematic of laboratory test cell

2. Schematic of heater and instrumentation located in the drift

3. Locations of the thermocouple placement along the primary fracture in Test 1 (a) and Test 2 (b)

4. Contours of temperature measured in the primary fracture after (i) 10, (ii) 50, and (iii) 110 days of heating for Test 1 (a) and after (i) 10, (ii) 50, and (iii) 140 days for Test 2 (b)

5. Locations of boiling isotherm in the primary fracture after 10, 20, 30, 50, 70, 90, 110, and 130 days of heating for Test 1(a) and after 10, 50, 90, 110, 150, 175, 200, and 210 days for Test 2 (b)

6. Temperature of drift air for Test 1 and for Test 2

7. Relative humidity of drift air for Test 1 and for Test 2

8. Photographs of the post-test drip sensors: Test 1, right side (a); Test 1, left side (b); Test 2, right side (c); Test 2, left side (d). The brown and white precipitate observed during Test 1 consisted of aphthitalite, barite, and calcite and was observed over 75 percent of the total length of the two drip-sensor sheets. Total corrosion of the sensor was observed at lower right of the right sensor. Precipitate consisting of aphthitalite and barite is observed over 100 percent of the total length of the two drip-sensor sheets in Test 2. There are multiple indications of total significant corrosion in Test 2.

9. Temperature measured at thermocouples 45, 56, and 63 during Test 2

10. Measured saturation of concrete samples collected from the test assembly at the conclusion of Test 2 from a midplane perpendicular to the drift (a) and near the test cell boundary perpendicular to the drift (b)

11. Electrical response from the eight segments of the drip sensors during Test 2

12. Schematic illustration of penetration of the boiling isotherm by flow down a fracture [adapted from Phillips (1996)]

13. Contours of matrix (a) and fracture (b) temperature numerically predicted for 10, 50, and 110 days of

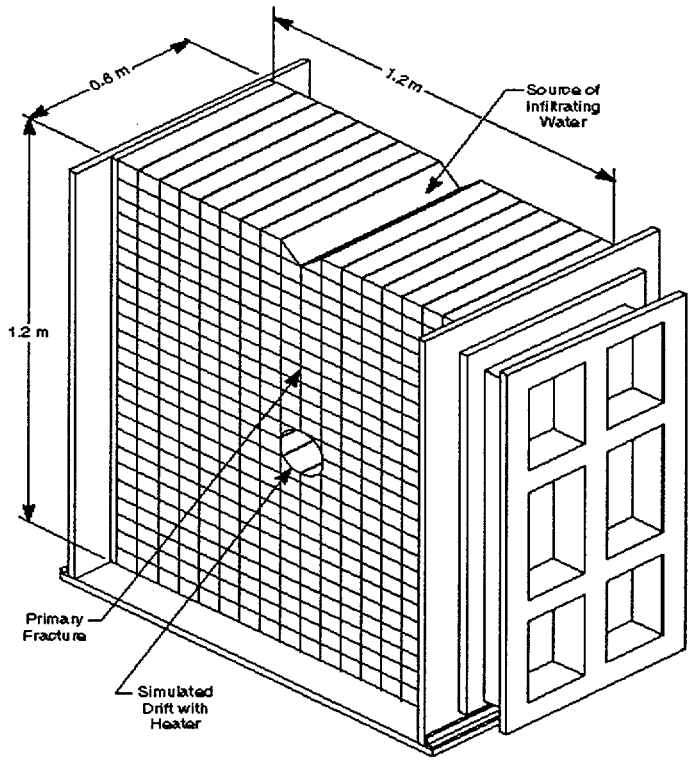
0.6 m
1.2m
Source of Infiltrating Water
1.2 m
Primary Fracture
Simulated Drift with Heater

Fig. 1

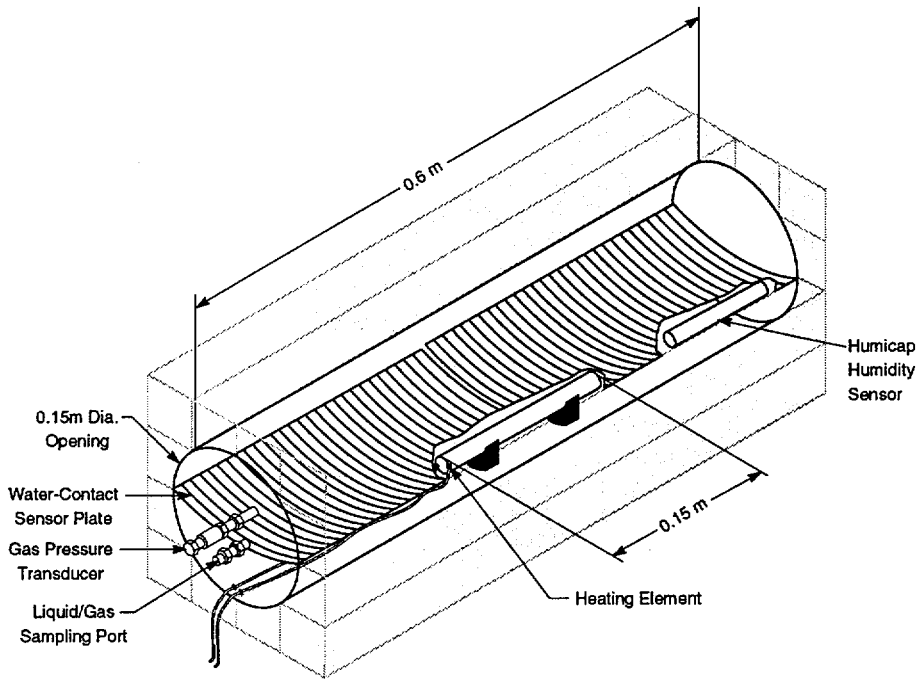
0.6 m
Humicap
Humidity
Sensor
0.15m Dia.
Opening
Water-Contact
Sensor Plate
Gas Pressure
Transducer
Liquid/Gas
Sampling Port
0.15 m
Heating Element

Fig 2

Test 1
Primary Fracture
Thermocouple Location

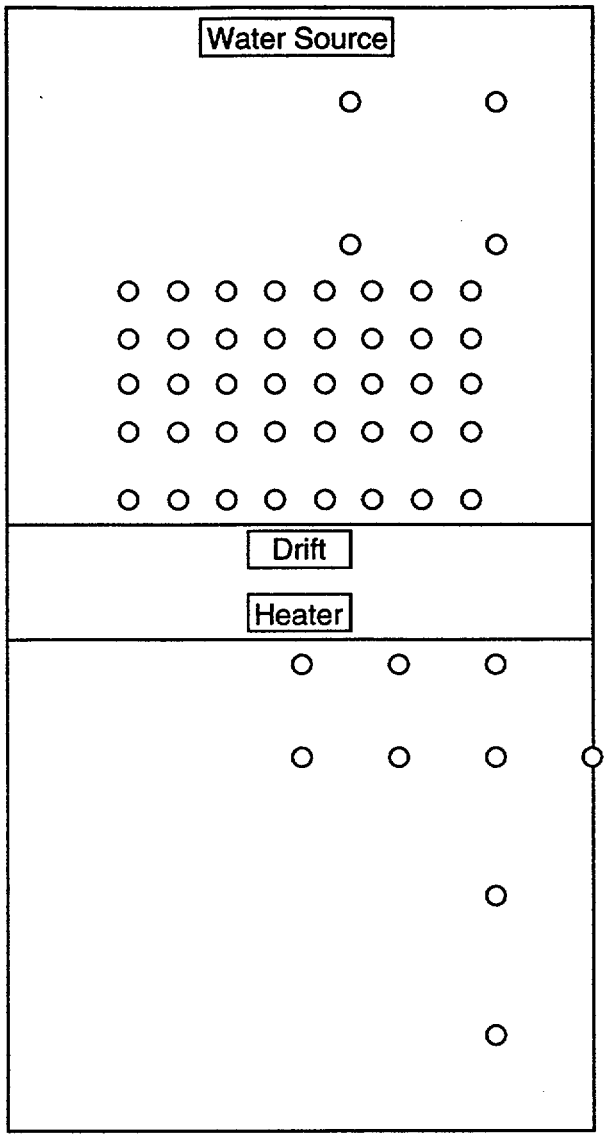

Test 2
Primary Fracture
Thermocouple Location

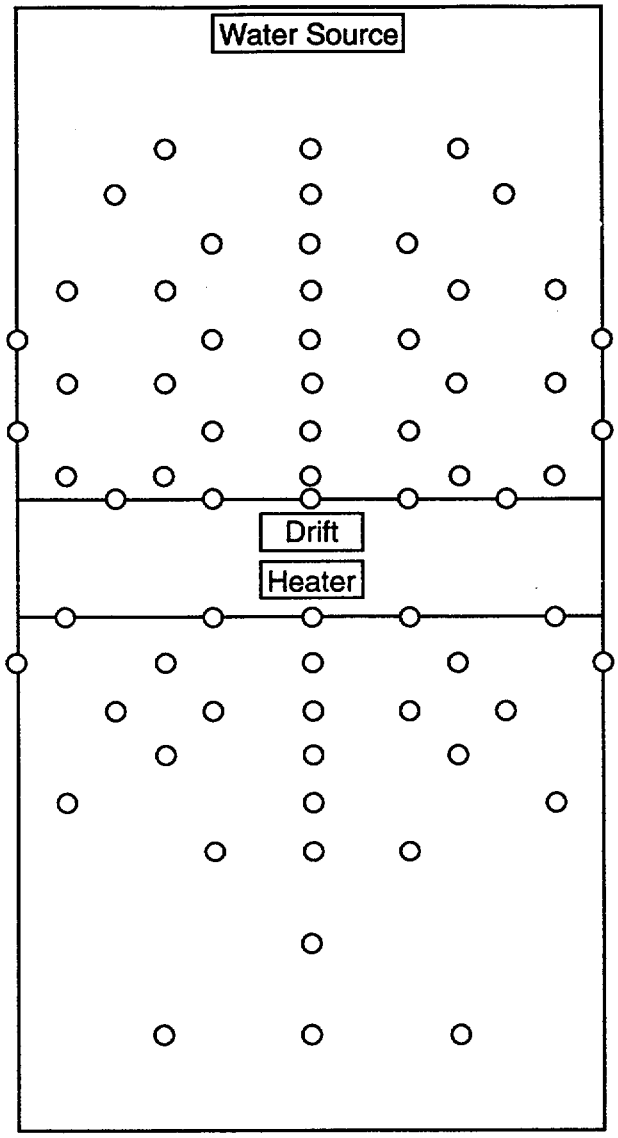

Fig 4

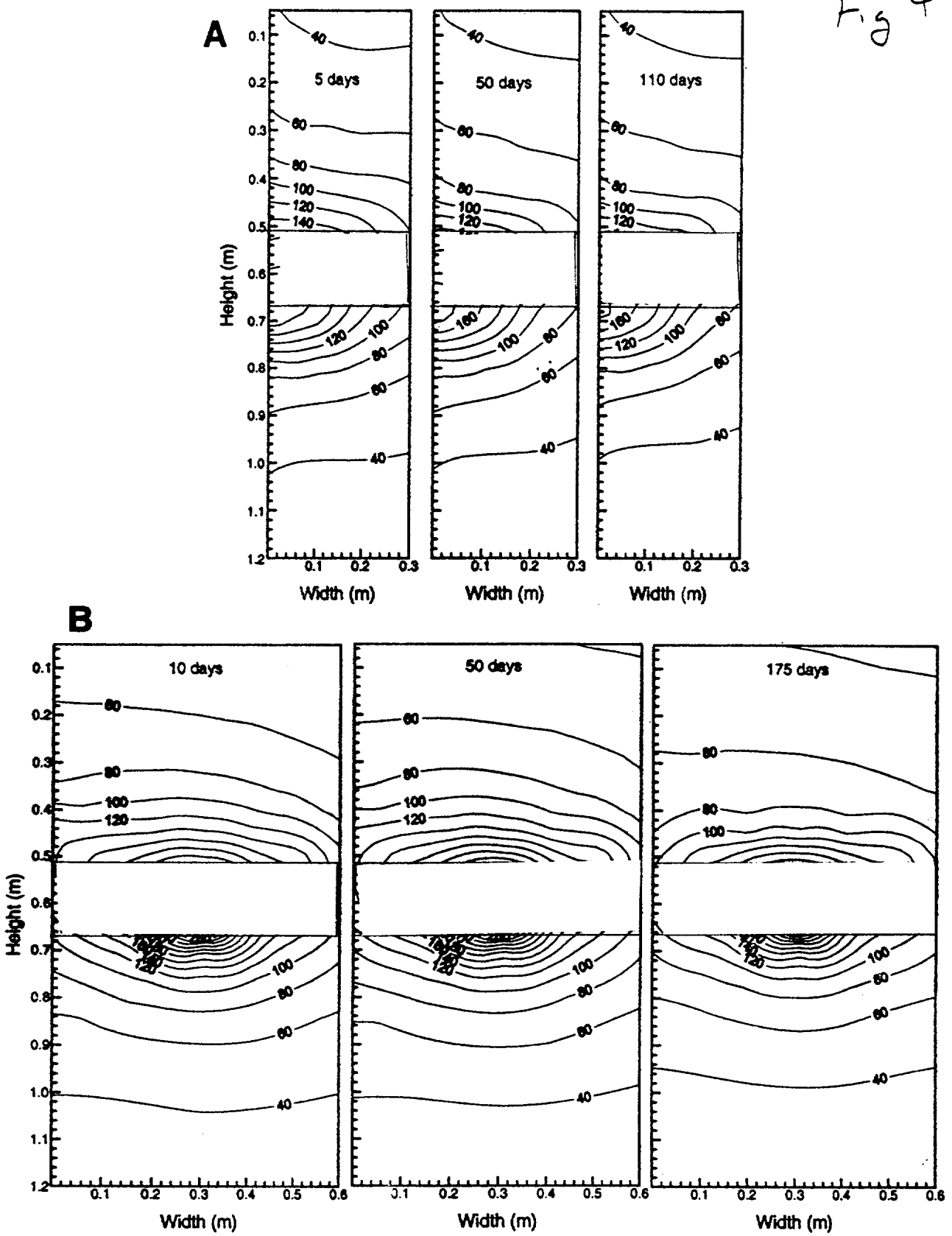
A
5 days
50 days
110 days
Height (m)
Width (m)
B
10 days
50 days
175 days
Height (m)
Width (m)

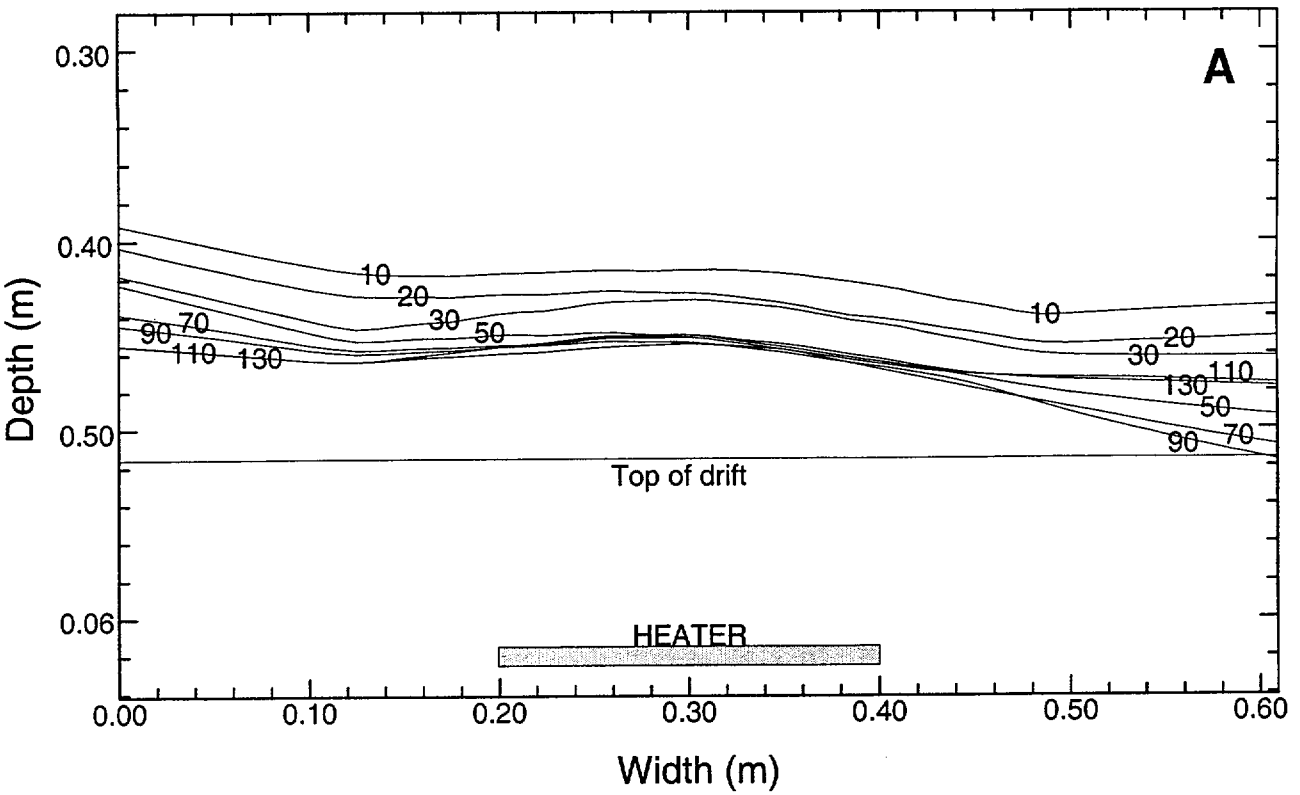
A
0.30
0.40
0.50
0.06
Depth (m)
10
20
30
50
90
70
110
130
10
30
20
130
110
50
90
70
Top of drift
HEATER
0.00
0.10
0.20
0.30
0.40
0.50
0.60
Width (m)

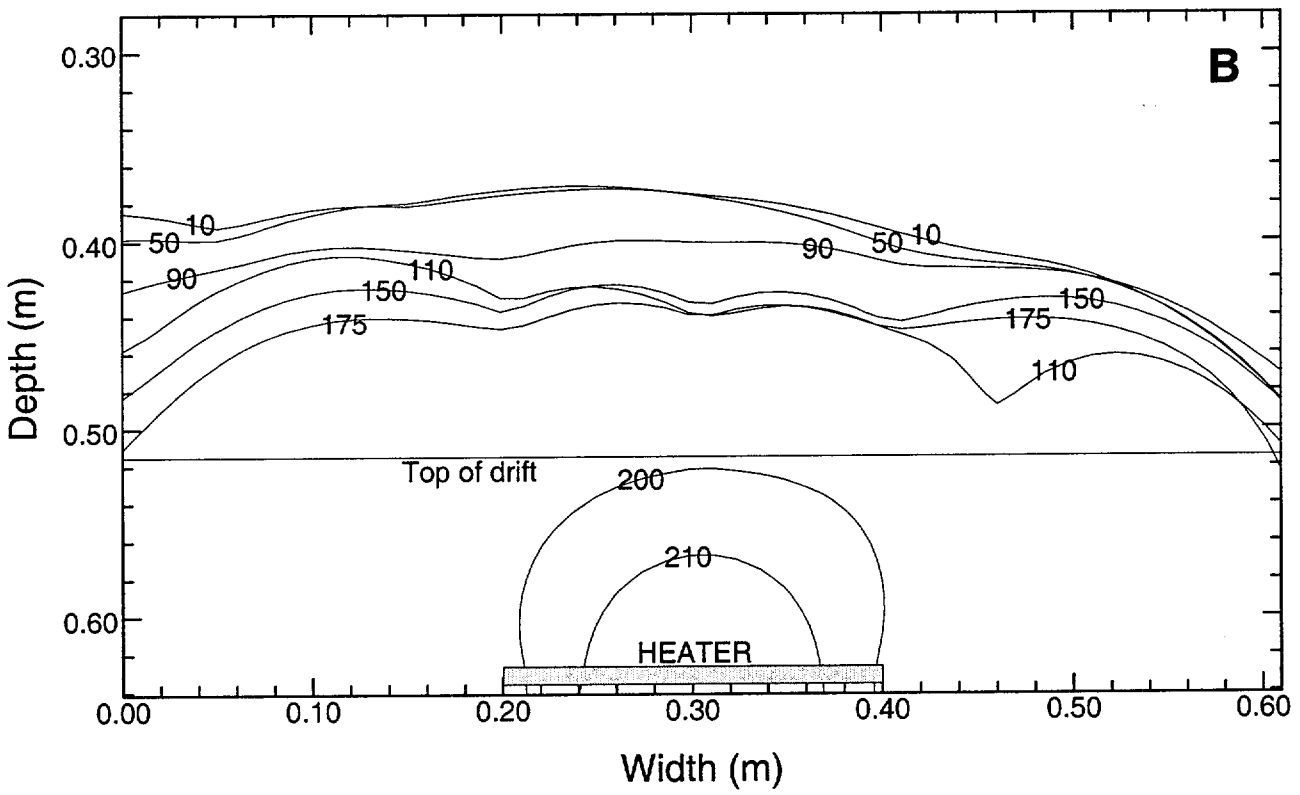
B
0.30
0.40
0.50
0.60
Depth (m)
10
50
90
110
150
175
90
50
10
150
175
110
Top of drift
200
210
HEATER
0.00
0.10
0.20
0.30
0.40
0.50
0.60
Width (m)

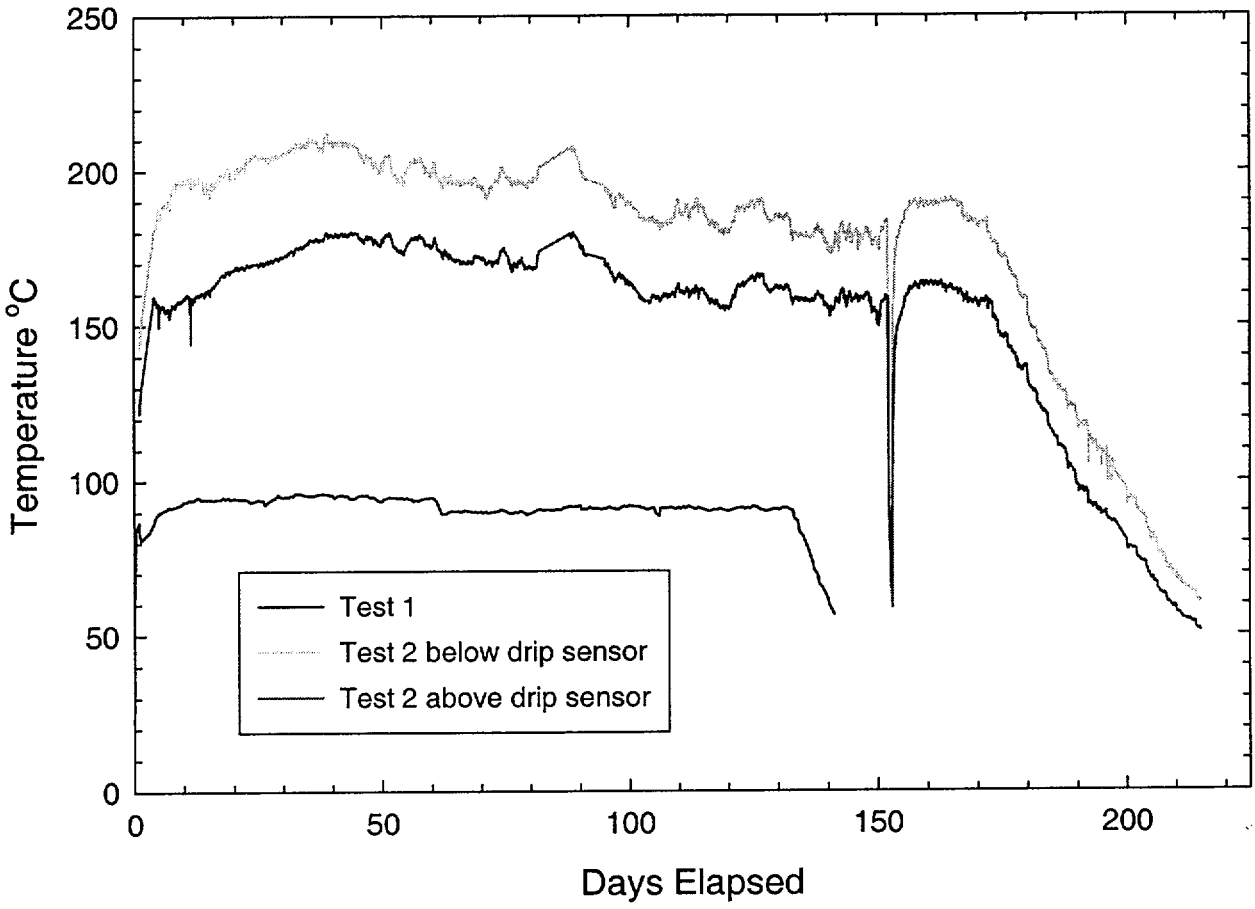
250
200
150
100
50
0
Temperature °C
0
50
100
150
200
Days Elapsed
Test 1
Test 2 below drip sensor
Test 2 above drip sensor

Fig 6

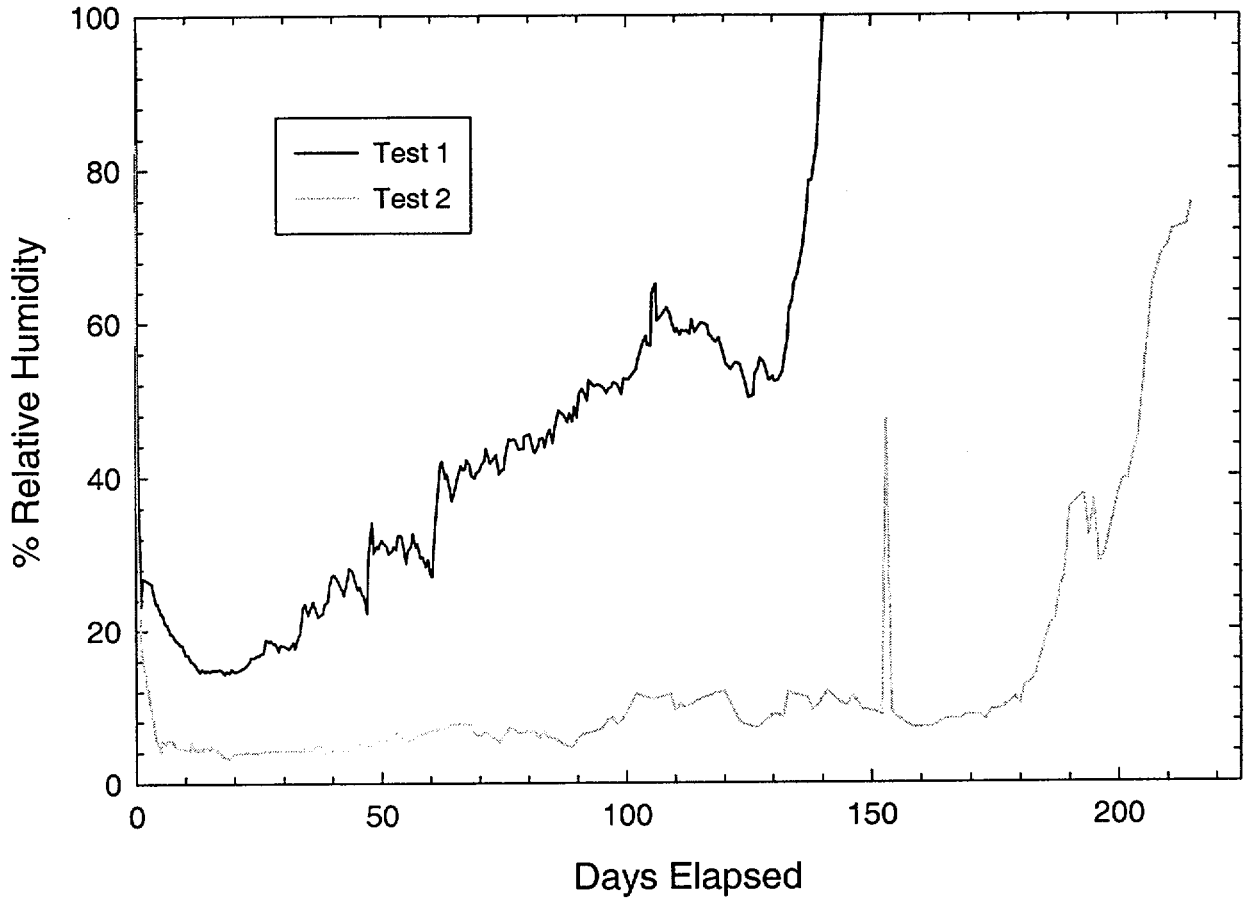
100
80
60
40
20
0
% Relative Humidity
Test 1
Test 2
0
50
100
150
200
Days Elapsed

Fig 7

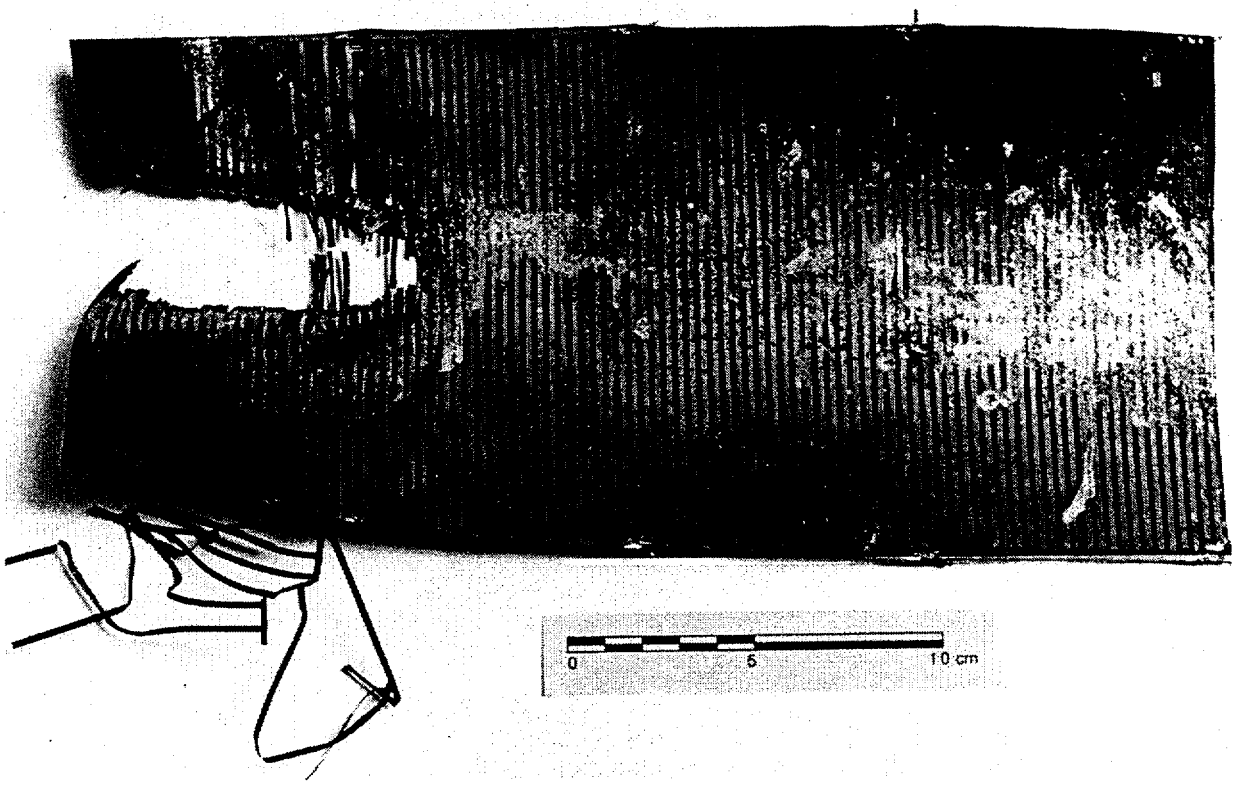

Test 1 Right

Fig 8(a)

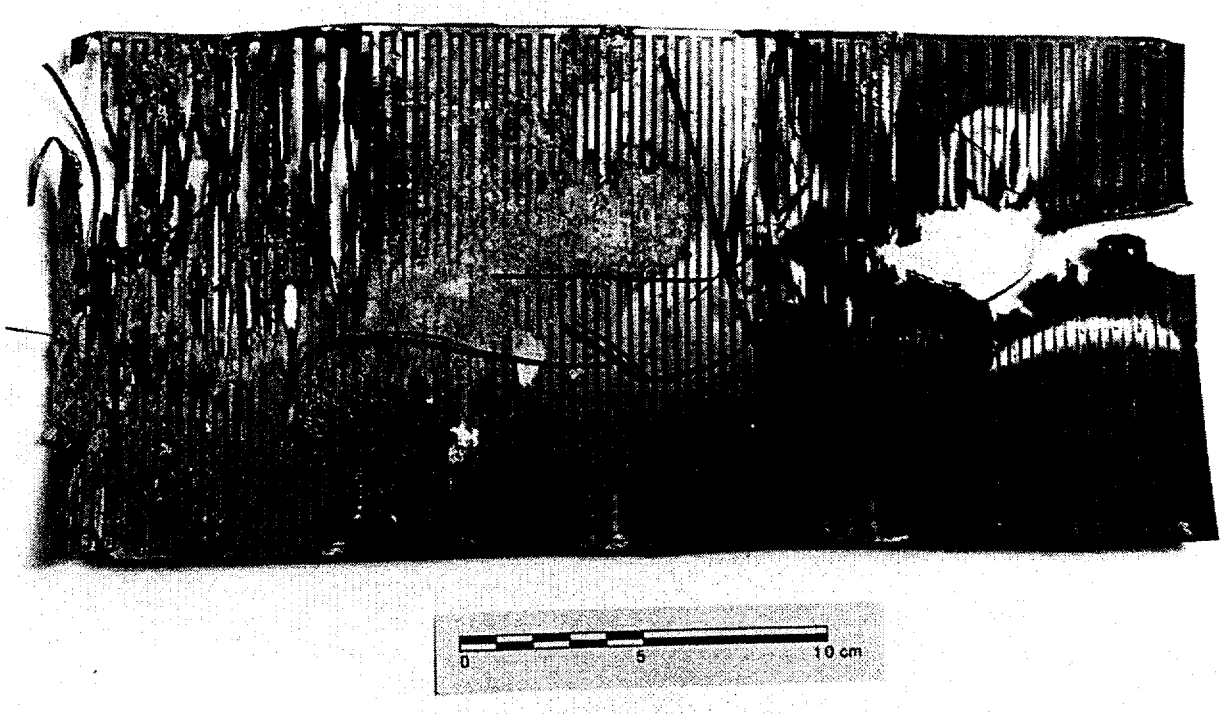

Test 1 Left

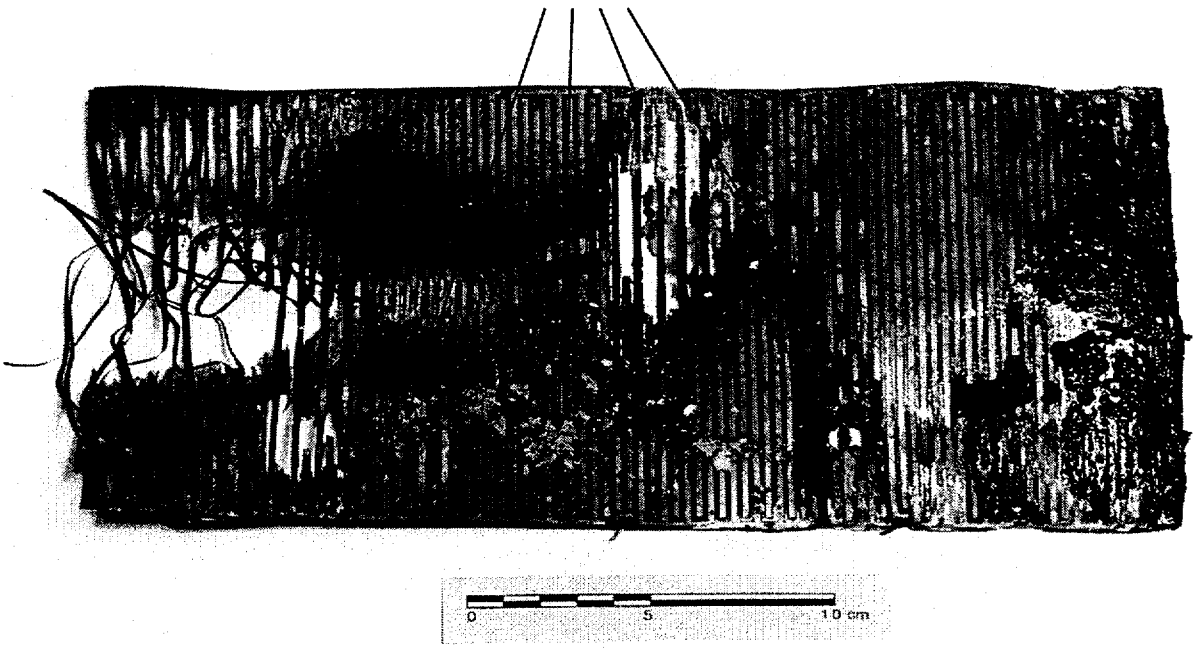

Test 2 right

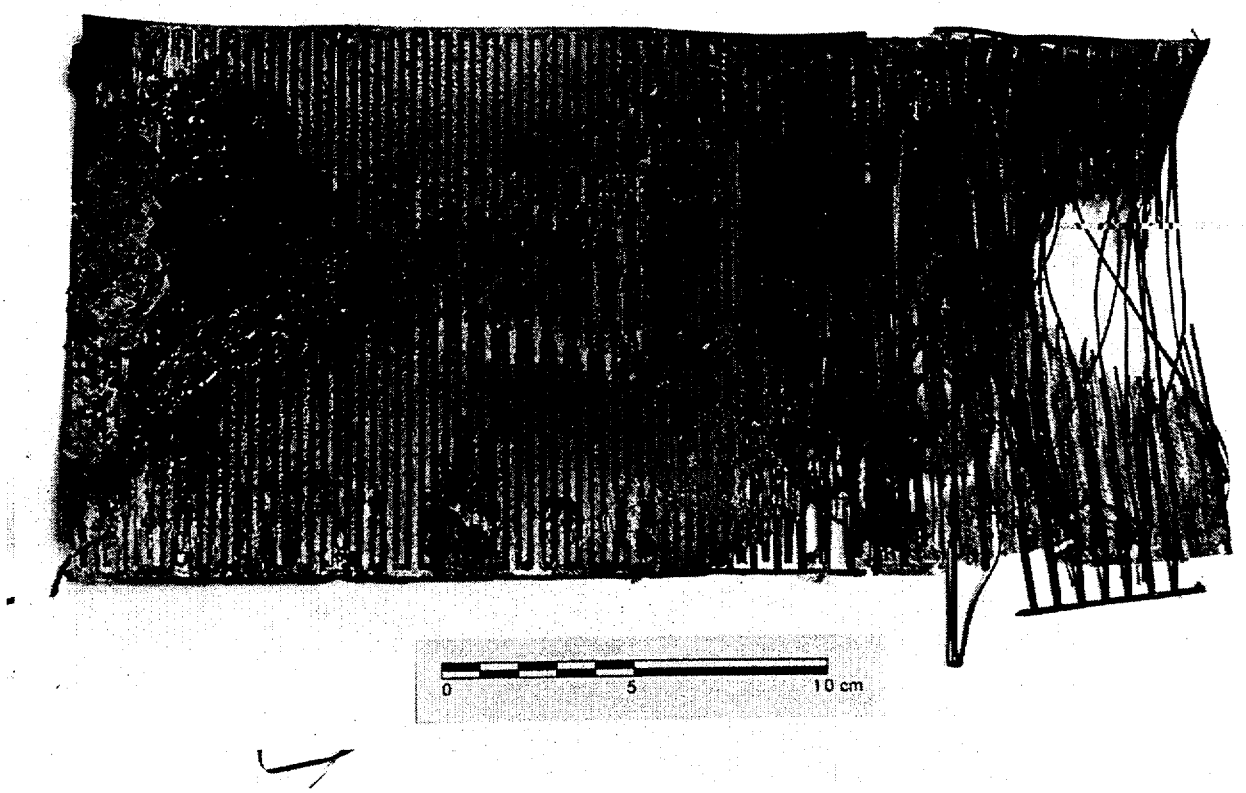

Test 2 Left

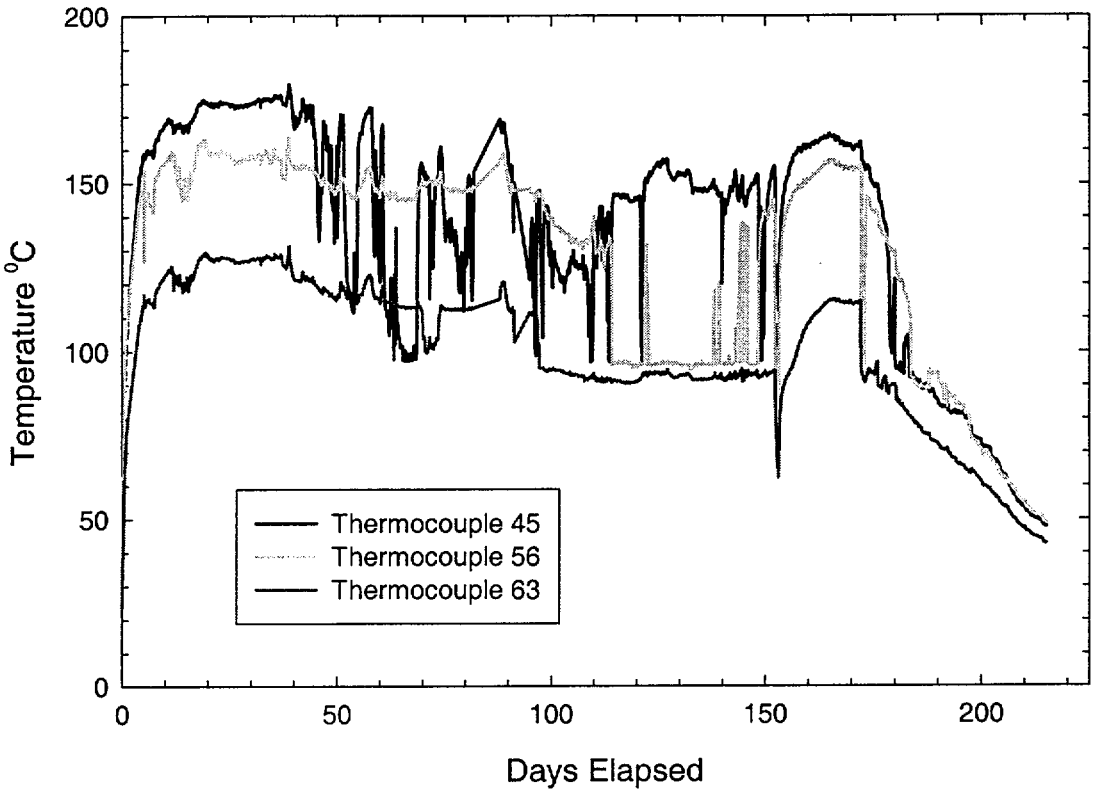
200
150
100
50
0
Temperature °C
0
50
100
150
200
Days Elapsed
Thermocouple 45
Thermocouple 56
Thermocouple 63

Fig 5

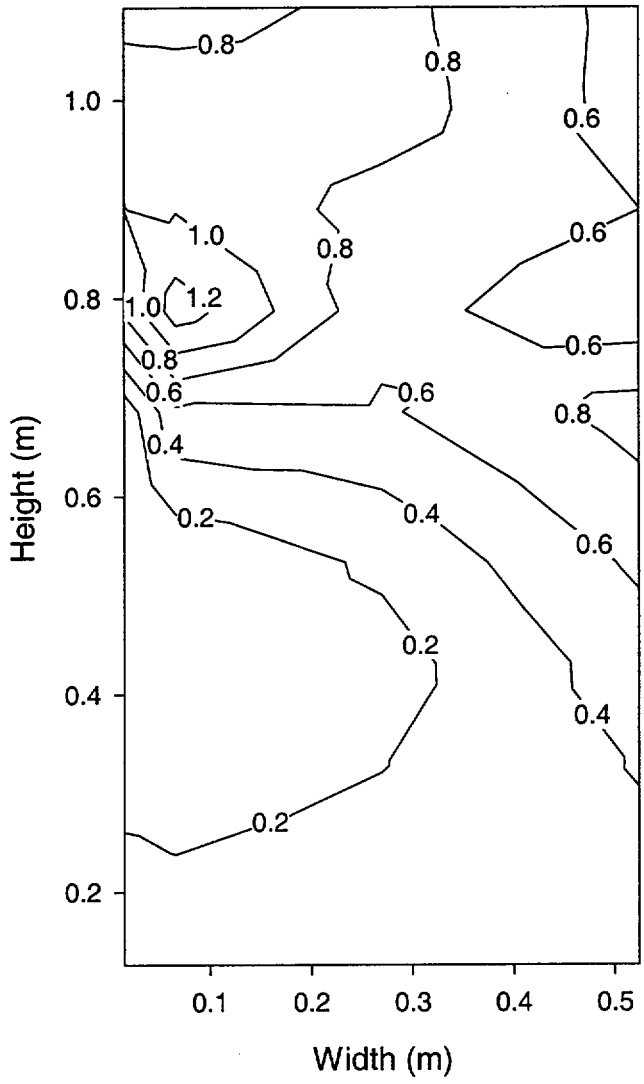
Height (m)
1.0
0.8
0.6
0.4
0.2
0.1
0.2
0.3
0.4
0.5
Width (m)
0.8
0.8
0.6
1.0
0.8
0.6
1.0
1.2
0.8
0.6
0.6
0.6
0.8
0.4
0.2
0.4
0.6
0.2
0.4
0.2

Fig 10(a)

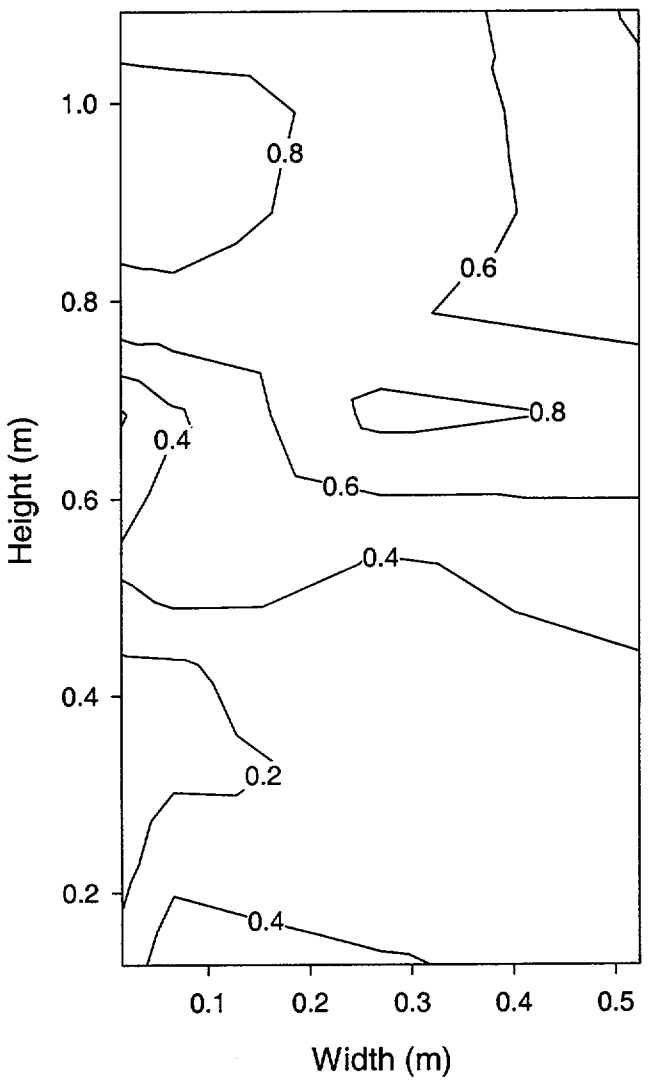

Fig 10(b)

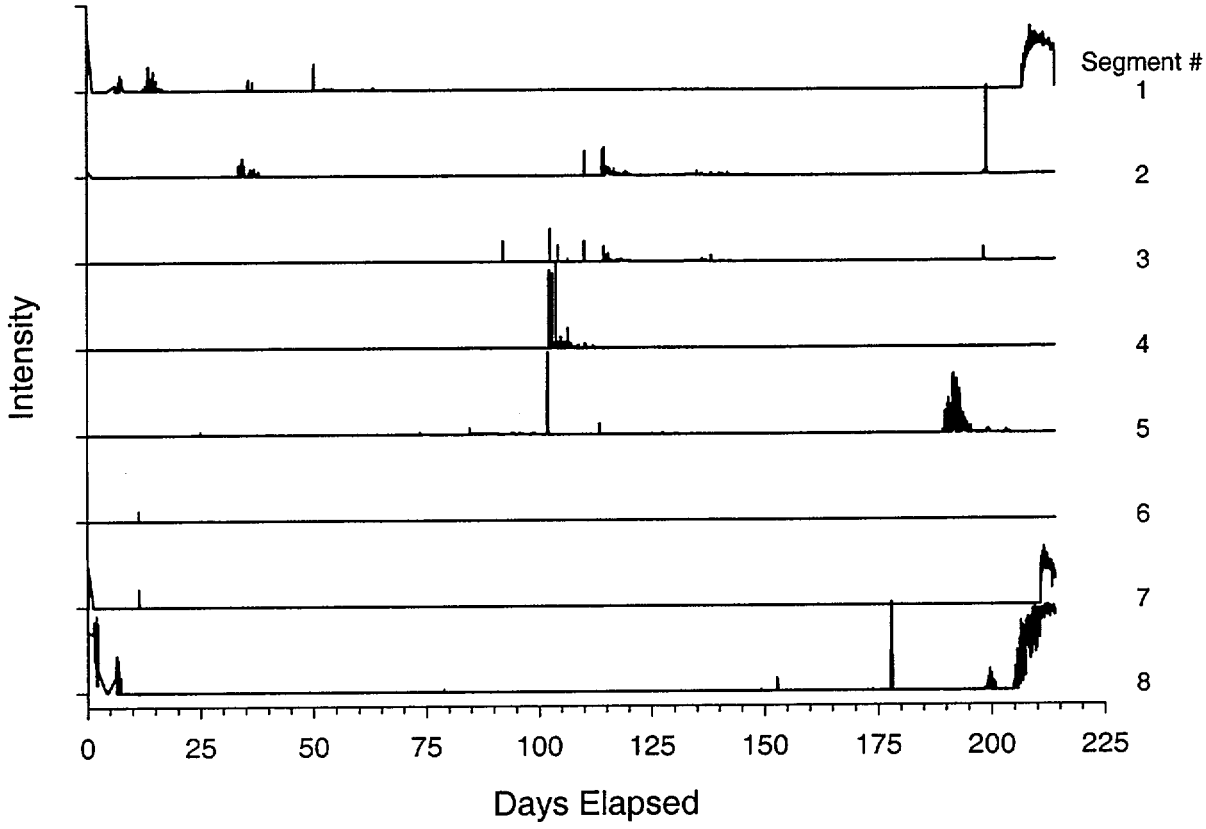
Segment #
1
2
3
4
5
6
7
8
Intensity
0
25
50
75
100
125
150
175
200
225
Days Elapsed

Fig 11

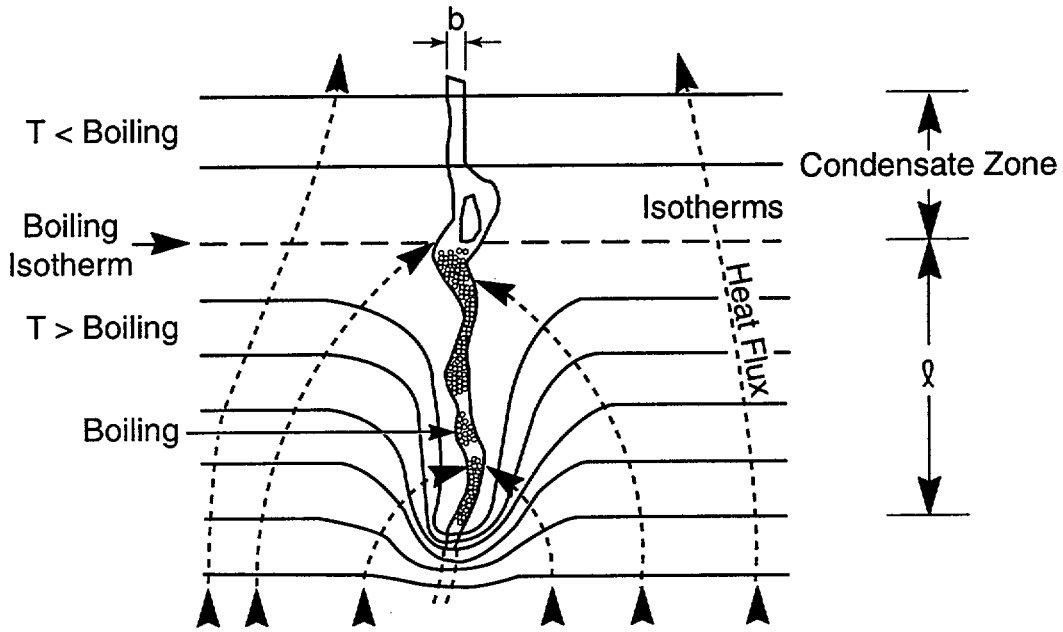
b
T < Boiling
Boiling
Isotherm
T > Boiling
Boiling
Isotherms
Heat Flux
Condensate Zone
ℓ

Fig 12

Test 1
[illegible]
[illegible]
[illegible]
[illegible]

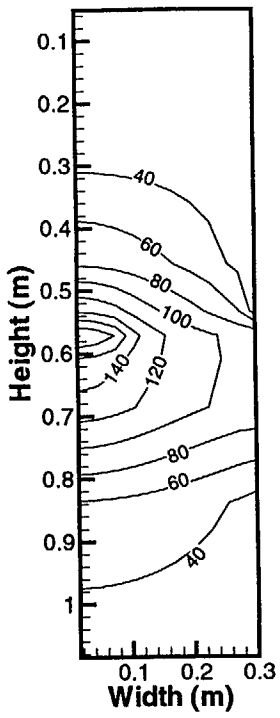

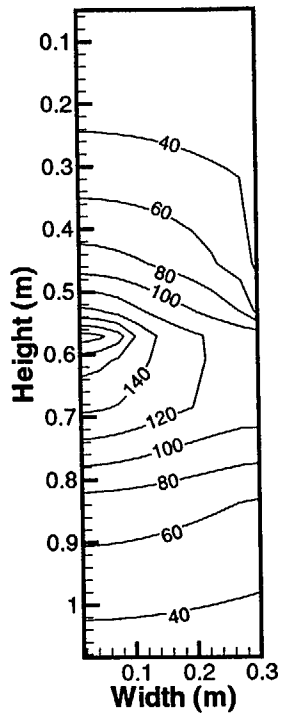

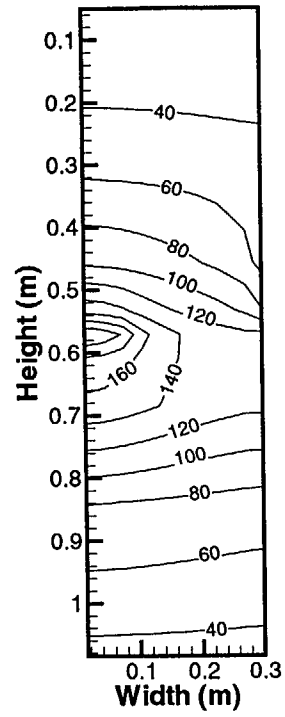

Fig 13(a)

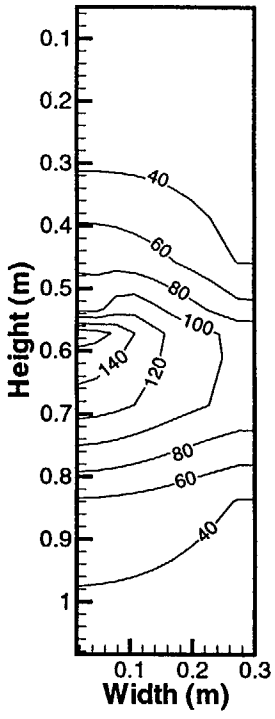

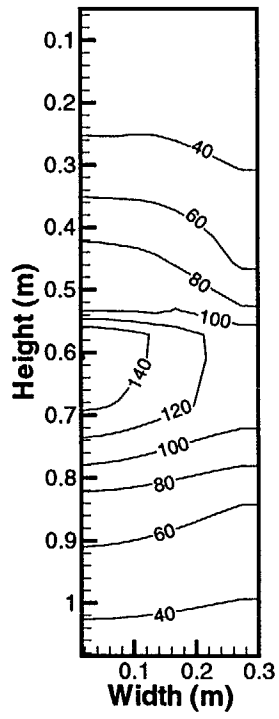

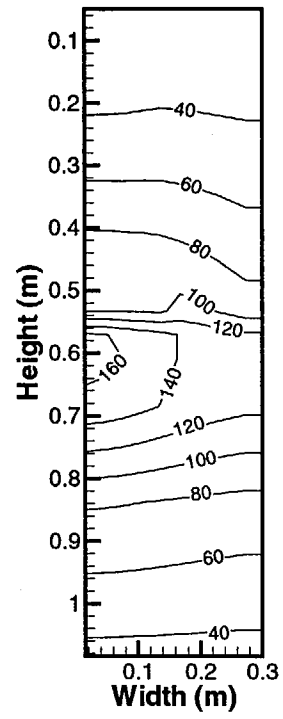

Test 1
por 50
sat 0.20
12, 50, 110
Fracture

Fig 13b

Test 2
pw 50
10, 50, 110
0.35
Matrix

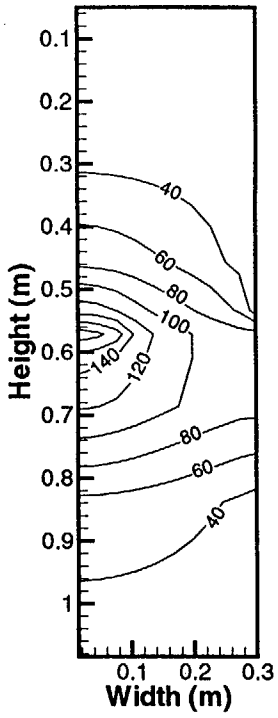

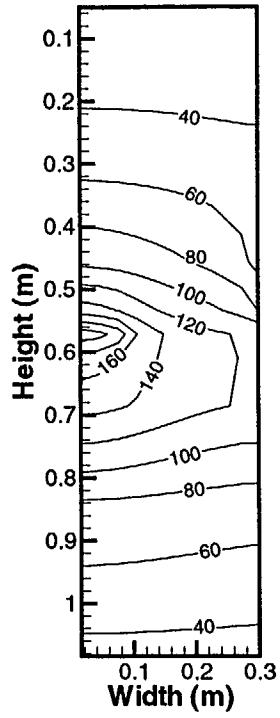

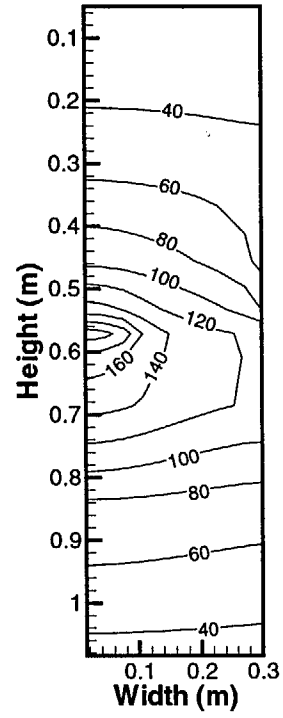

Fig 14(a)

Test 2
Por 50
Frac

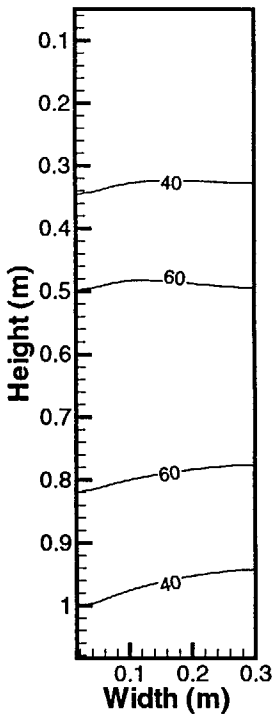

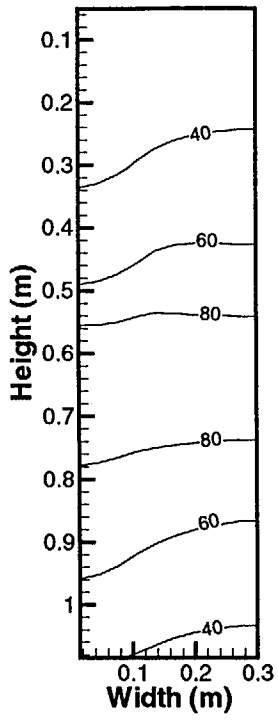

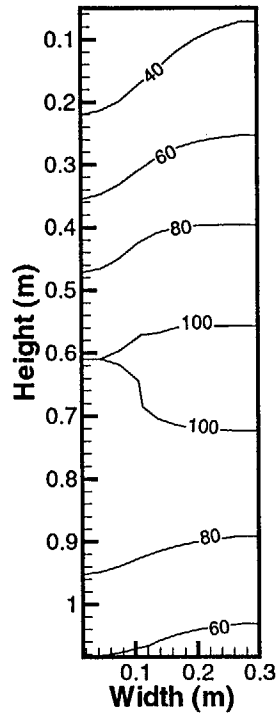

Fig 14(b)

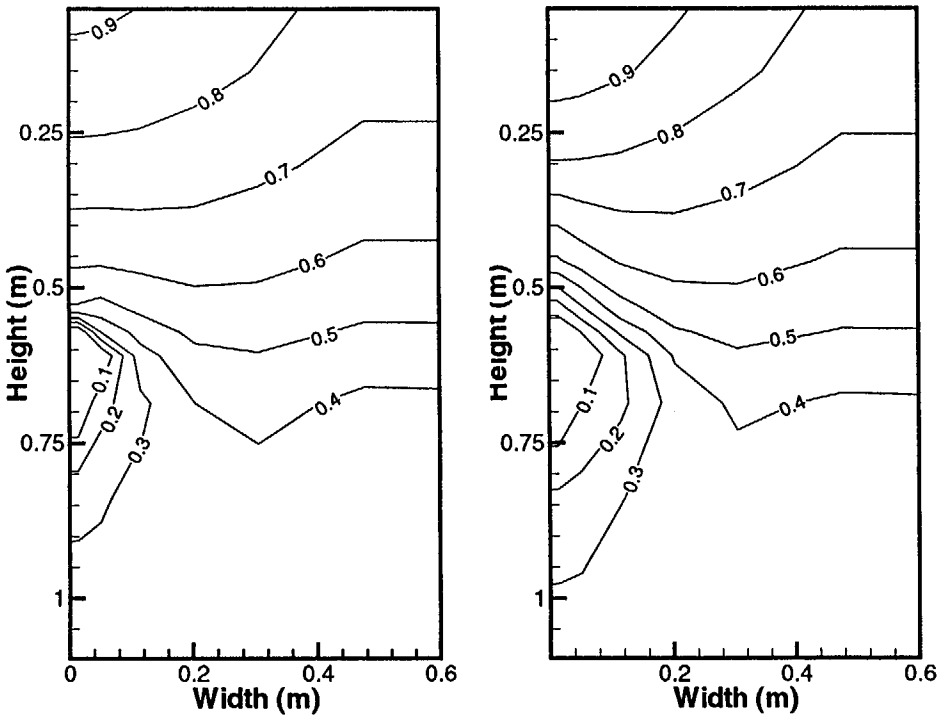

Fig 15 (a) & (b)

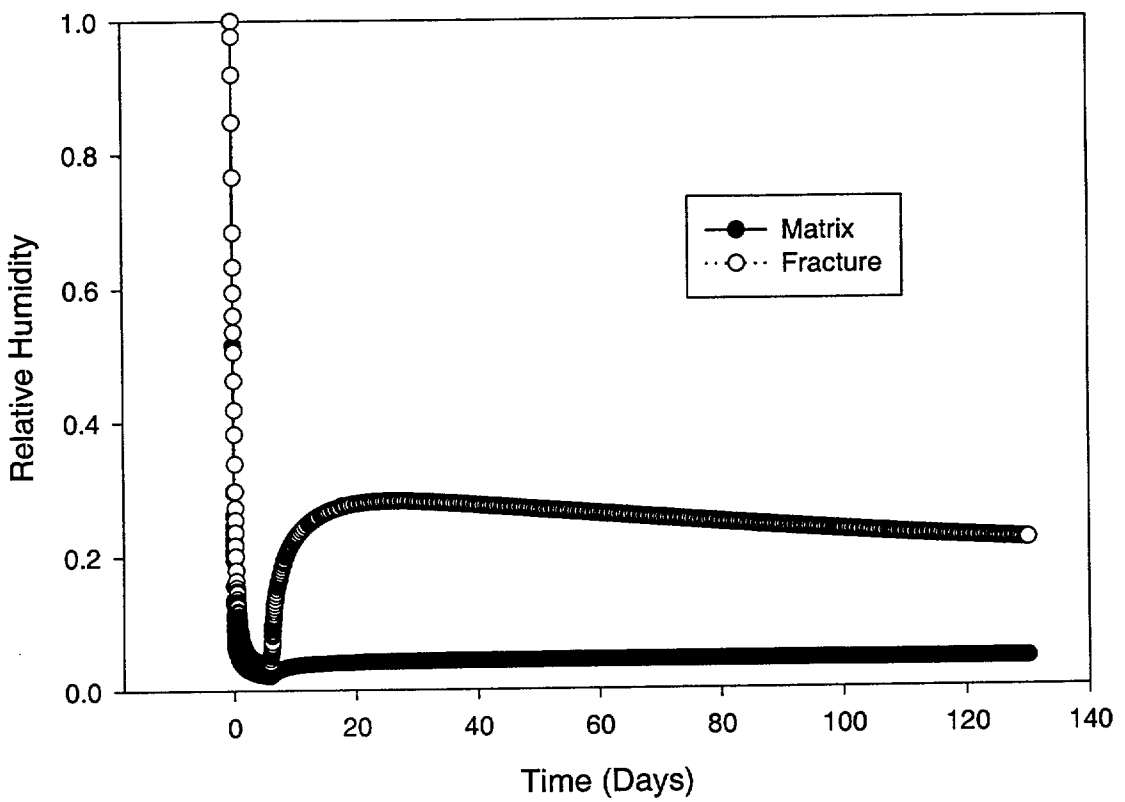

Test 1

Fig 16(a)

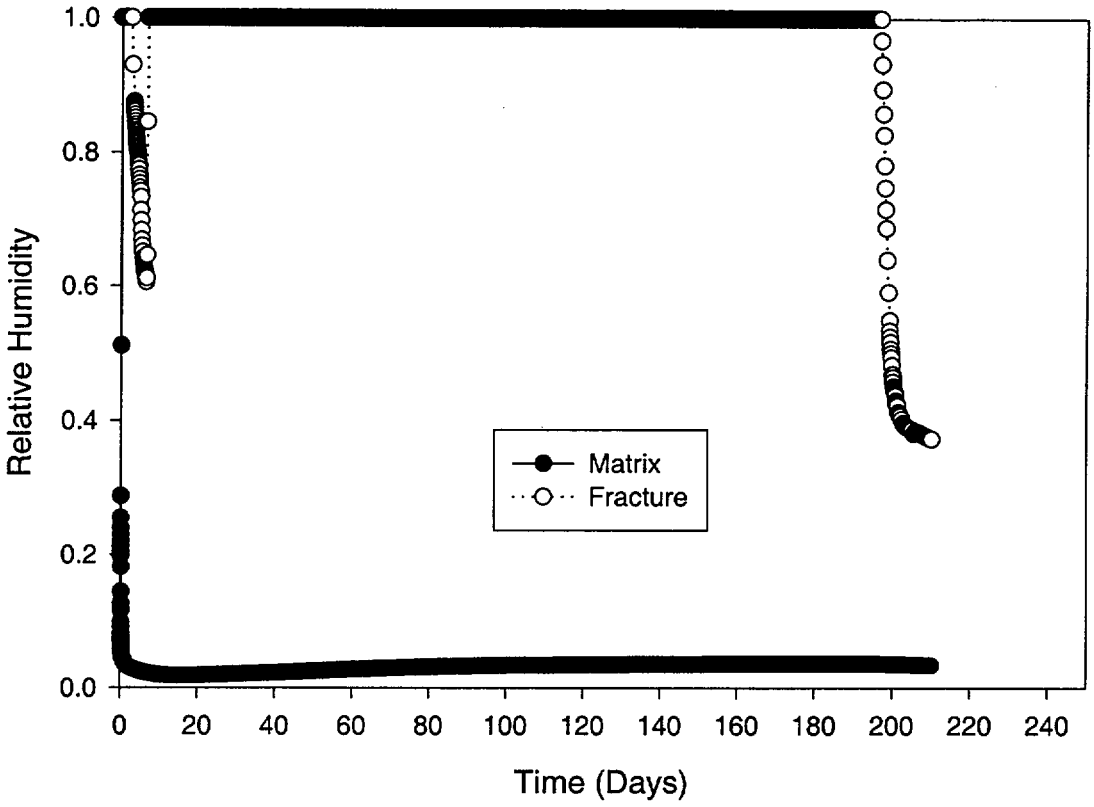

Test 2

Fig 16 (b)